CONTRIBUTIONS OF

THE OBSERVATORY

OF NEW MEXICO STATE UNIVERSITY

LAS CRUCES, NEW MEXICO

88003

Volume 1 April, 1976 Number 4

Published by: The Astronomy Department
Box 4500, New Mexico State University
Las Cruces, New Mexico 88003

This issue completes Volume 1. Future issues will bear the serial number only, starting with the Number 5.

CONTRIBUTIONS OF

THE OBSERVATORY

OF NEW MEXICO STATE UNIVERSITY

LAS CRUCES, NEW MEXICO

88003

Volume 1 April, 1976 Number 4

Published by: The Astronomy Department
Box 4500, New Mexico State University
Las Cruces, New Mexico 88003

This issue completes Volume 1. Future issues will bear the serial number only, starting with the Number 5.

CONTRIBUTIONS OF THE OBSERVATORY, NEW MEXICO STATE UNIVERSITY

Volume 1, Number 4 April 1976

TABLE OF CONTENTS

Published by: Astronomy Department
Box 4500, New Mexico State University
Las Cruces, New Mexico 88003

This issue completes Volume 1. Future issues will bear the serial number only, starting with Number 5.

NON-LTE PROFILES OF STRONG SOLAR LINES

T. J. Schneeberger and H. A. Beebe

Department of Astronomy

New Mexico State University, Las Cruces, N.M. 88003

Abstract

The complete linearization method is applied to the formation of strong lines in the solar atmosphere. Transitions in Na I, Mg I, Ca I, Mg II and Ca II are computed with a standard atmosphere and microturbulent velocity model. The computed profiles are compared to observations at disk center.

Key Words: Solar Lines, Non-LTE

I. Introduction

Homogeneous empirical models of the solar atmosphere show in terms of a spatially averaged atmosphere a positive temperature gradient in the upper layers, the solar chromosphere. The radial level at which the gradient reverses sign is by definition the region of the solar temperature minimum, but the physical conditions in that region are not well determined. Papers describing empirical models such as the Harvard Smithsonian Reference Atmosphere, hereafter called the HSRA (Gingerich et al., 1971) refer to this difficulty with respect to model construction and available observations. In addition, recent theoretical predictions of core profiles of strong spectral lines have shown somewhat conflicting results. Shine, Milkey, and Mihalas (1974) in a study of the Ca II H and K lines using

Non-LTE theory and a photon redistribution function which allows coherence outside of the Doppler core, show that calculated K I and H I features can be well matched with observations with a temperature minimum several hundred degrees above the HSRA values. However, Altrock and Canfield (1974) are able to match Mg I strong line core profiles with a Non-LTE approach applying complete redistribution of photons in the line, with a temperature-height relation very similar to that of the HSRA.

In this study we calculate the core intensity profiles of six strong lines of four ionic species using Non-LTE theory, complete redistribution of photons in the line, and the HSRA. The investigation is, in fact, a standardization of a technique that we intend to apply to future work which will include the effects of inhomogeneities on the line core profiles. Thus we do not expect the calculated profiles to match the observations but we do intend to derive information from the study about the atmospheric model, atomic models and the applicability of the complete redistribution function to the formation of the several lines.

We describe the method of calculation in Section II, and give a brief description of the model atmosphere and microturbulence model adopted for this study in Section III. In Section IV we describe the model atoms, listing wavelengths of line centers, atomic parameters and electron collisional and photon cross-sections for the various transitions used in the calculations. We discuss the results in Section V.

II. Method of Calculation

In this study we apply the complete linearization method as applied to Non-LTE transfer problems developed by Auer, Heasley and Milkey (1972).

The method includes complete redistribution of photons in bound-bound and bound-free transitions where the problem is solved "in detail", that is, where we solve the transfer equations for the transition. The computer codes described by Auer, Heasley and Milkey, hereafter called AHM, and as revised at NMSU, also allow depth variation of line broadening parameters such as microturbulence and Van der Waals broadening as well as temperature, density and continuous opacities.

The AHM allows transitions not done in detail to be included with the assumption of detailed balance or by dilution. The second method specifies a radiation temperature T_{RAD} for the given transition, in which the temperature is set equal to T_e, the local electron temperature, at all depths or set equal to a constant T_{RAD} above points optionally either in the photosphere or chromosphere at which $T_e = T_{RAD}$. The options are discussed further in AHM.

The physical formulation of the Non-LTE method has been discussed in considerable detail elsewhere (Athay and Skumanich, 1967) and briefly in an earlier contribution of this series (Beebe and Hollars, 1973).

Intensities in the line are calculated independently by transferring line source functions, line center and continuum optical depths and line formation parameters to program PROFILE. This program calculates line absorption coefficients for an arbitrary set of wavelengths near line center and assumes an LTE source function for the continuum. PROFILE has been tested satisfactorily against analytic source functions with known solutions and for self consistency with respect to depth point spacing.

III. The Model Atmosphere

In this study we have used the HSRA model exclusively. We interpolate 56 depth points appropriate to the entire range of line formation from the 95 which characterize the model. The departure coefficients for the ground state of hydrogen are included as listed in the HSRA.

Microturbulent velocities are included in the model, derived from recent line profile calculations. V_T vs. depth models are plotted in Figure 1 for several successful applications (Altrock and Canfield, 1974, Lites, 1973, and Linsky and Avrett, 1970). The values were averages of the horizontal and vertical components of the anisotropic models. The adopted model follows that of Lites in the photosphere and the Linsky-Avrett model in the chromosphere, and bears a close resemblance to the model proposed by Unno (1959).

IV. Atomic Data

Atomic models and corresponding physical data for Na I, Mg I, Ca I, Mg II and Ca II are described in the following paragraphs.

a) Na I

A model atom consisting of the 3s $^2S_{1/2}$, 3p $^2P^o_{1/2}$, 3p $^2P^o_{3/2}$, 3d $\overline{D}$ and continuum levels has been adopted for this study. The 3d $^2D_{3/2}$ and

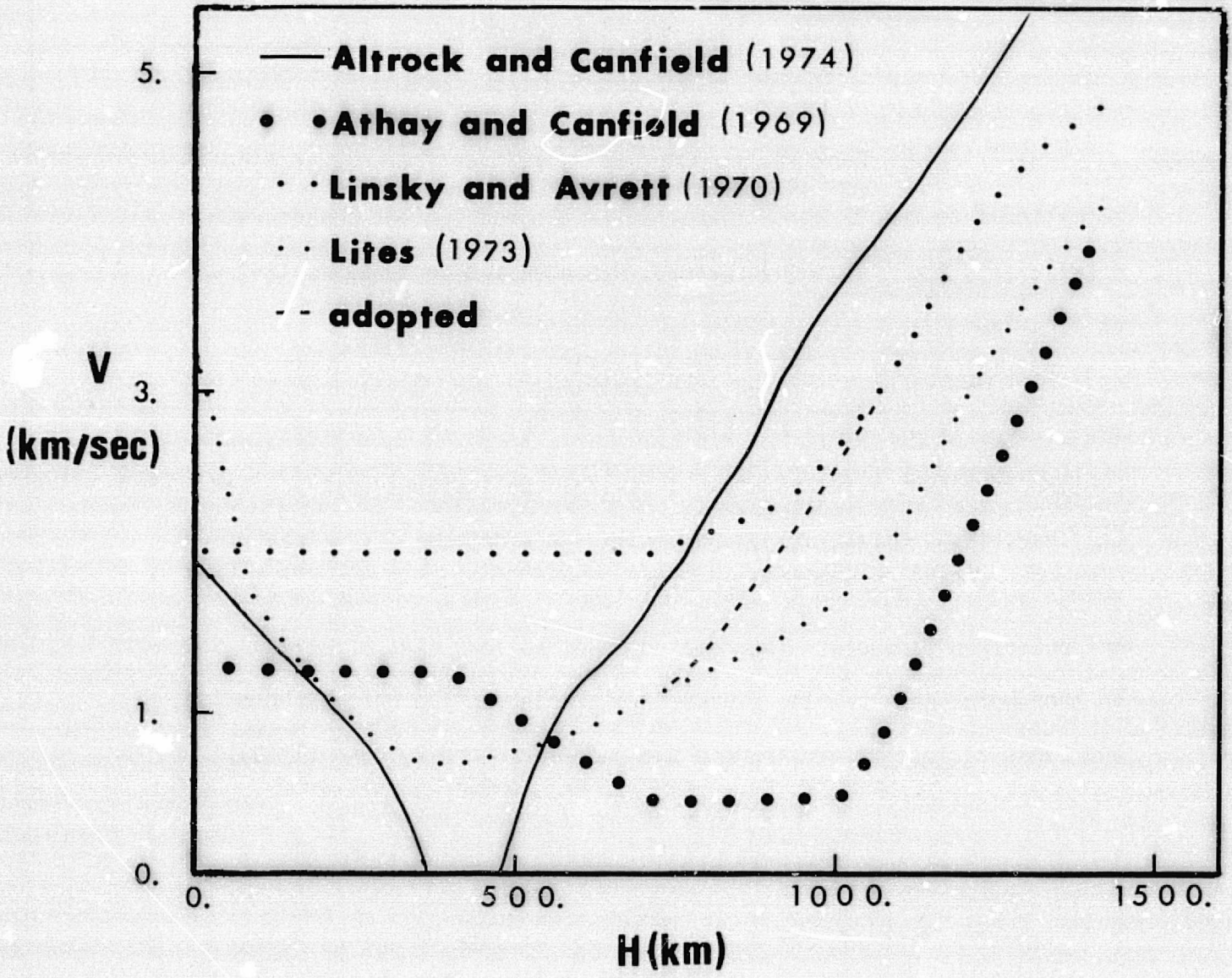

Fig. 1. Microturbulence models, velocity (km/sec) vs. height (km). Height is defined as in the HSRA. The adopted model follows Lites' in the photosphere and low chromosphere, and is the joined via the dashed line to the Linsky-Avrett model.

$3d\ ^2D_{5/2}$ levels of Na I have been represented here by an average level 3d $\overline{D}$ with a statistical weight of 10. Athay and Canfield (1969) have previously used this model atom. We have computed the D_1, D_2, and 8194.78 Å line transitions in detail. The oscillator strengths for these and all other lines discussed in this study were obtained from Wiese et. al. (1969), unless otherwise noted. Fixed rates described by radiation temperatures T_{RAD} were used for all free-bound continua. We have used the radiation temperatures, collisional cross sections, and photoionization cross sections listed by Athay and Canfield (1969).

The abundance of Na relative to hydrogen by number is 1.78×10^{-6}, from Allen (1973). The Van der Waals dispersion constant, C_H, was taken to be 7.3×10^{-32} for the D_1 and D_2 transitions. This value of C_H was assumed for the 8194 Å transition also.

b) Mg I

We have used the Mg I model atom described by Altrock and Canfield (1974). This model consists of the $3s^2\ ^1S_0$, $3p\ ^3P^o_1$, $3p\ ^1P^o_1$, $4s\ ^3S_1$, and continuum levels. Detailed calculations were made for the forbidden transition at 4571.1 Å, the resonance transition at 2852.1 Å and the b_2 transition at 5172.7 Å. The oscillator strength of the forbidden 4571 Å transition was taken to be 4.3×10^{-6}. Fixed rates described by radiation

temperatures have been used for all bound-free continua. Altrock and Canfield (1974) give the values of T_{RAD}, collisional cross sections, and photoionization cross sections and these were adopted for our calculations. The Mg I bound-free opacities included as background opacities in the linear code were deleted unless the opacity was not included in the model atom calculations.

The abundance of Mg relative to hydrogen by number is set at $3. \times 10^{-5}$, following Altrock and Canfield (1974). The Van der Waals dispersion constant for the 4571 Å and 2852 Å transitions equals 5.5×10^{-33}, from Weideman (1955). The wings of the b_2 line require a relatively large value of C_H to produce the observed profile, and $C_H = 3. \times 10^{-31}$ was found to be necessary in this work.

c) Ca I

A simple two level plus continuum representation was adopted for the neutral calcium atom. This model includes the $4s^2\ {}^1S_o$, $4p\ {}^1P^o_1$, and continuum levels. The resonance line 4226.7 Å was calculated in detail and the bound-free continua were calculated with fixed rates set by radiation temperatures. We have taken $T_{RAD} = 5550.°K$ for the 4S → continuum transition, and $T_{RAD} = 5000.°K$ for the 4P → continuum transition. The photoionization cross sections were both set at $1. \times 10^{-18}$ cm^2 (Lites, 1973). The collisional rate from the 4S to the 4P level was calculated from experimental data of Crandall et. al. (1974).

The calcium abundance relative to hydrogen by number derived by Lambert and Warner (1968), 2.14×10^{-6}, was adopted for this study. The Van der Waals dispersion constant was inferred from the work of Lites (1973), $C_H = 4. \times 10^{-32}$.

d) Ca II

Three levels plus a continuum were included in the Ca II model. The bound levels are 4s $^2S_{1/2}$, 3d $^2D_{5/2}$ and 4p $^2P^o_{3/2}$. Detailed calculations were made for the K line, 3933.0 Å, the infrared triplet line at 8452.1 Å, and the 4s $^2S_{1/2}$ → continuum transition. A ν^{-3} dependence was assumed for the continuum transition, and the photoionization cross section at the continuum head was taken to be 1.1×10^{-18} cm^2. The remaining free-bound continua were computed with fixed rates, with T_{RAD} = 5000°K. The photoionization cross sections and collisional cross sections were adopted from Auer, Heasley, and Milkey (1972). The Van der Waals dispersion constant for both line transitions was set at 1.3×10^{-32} (Weideman, 1955).

e) Mg II

The h and k lines of Mg II were calculated in detail utilizing the model atom and atomic data of Milkey and Mihalas (1974). This model includes the 3s $^2S_{1/2}$, 3p $^2P^o_{1/2}$, 3p $^2P^o_{3/2}$ and continuum levels. Fixed rates were used for the bound-free continua. Radiation temperatures, photoionization cross sections and the collisional rate equations are from Milkey and Mihalas (1974). Dumont (1967) gives a Van der Waals dispersion constant, $C_H = 5. \times 10^{-33}$, and this value was adopted for the h and k lines.

V. Results and Discussion

The Kitt Peak Solar Atlas (Brault and Testerman, 1972) provides observed profiles at disk center for many of the lines included in this study. We have visually smoothed over absorption lines due to other transitions which occur in the observed profiles of the lines of interest. Figures 2 through 6 compare these observations to the computed profiles of

Na I λ5890., Ca I λ4227., Mg I λ5172., Ca II λ3933., and Ca II λ8542., respectively, at disk center.

The cores of the D_2, λ4227, and b_2 transitions are formed in the lower chromosphere. The line center optical depths, τ_o, become equal to unity for these transitions at temperatures and heights above the temperature minimum. We have $\tau_o(5890) = 1$ at $T_{HSRA} = 5200°K$, $\tau_o(4227) = 1$ at $T_{HSRA} = 5000°K$ and $\tau_o(5172) = 1$ at $T_{HSRA} = 4700°K$. The computed cores of these lines are darker than observed. It is well known that the microturbulent velocity gradient can effect the core brightness of lines and preliminary calculations with Ca I indicate that a microturbulence model with a steep gradient similar to that used by Altrock and Canfield (1974) (see Figure 1) will produce the observed core intensity of λ4227. at $\mu = 1.0$. The computed Doppler cores are wide compared to observations for both Ca I and Mg I.

The wings of D_2, λ4227., and b_2 are in reasonable agreement with observation. Tests with Mg I λ5172 have shown that the agreement can be improved by judicious adjustment of a single parameter, the Van der Waals constant. As found by Athay and Canfield (1969), the Mg I b lines require a Van der Waals constant which is substantially larger than theoretically predicted in order to match the broad wings of these lines.

Figure 5 compares the computed and observed profiles at disk center for the Ca II K line. Except for satisfactory agreement at K3, the profiles are widely discrepant. This may be due to the neglect of coherency effects (see Shine, Milkey, and Mihalas, (1975)) or to the neglect of the inhomogeneous structure of the chromosphere (Beebe, 1971).

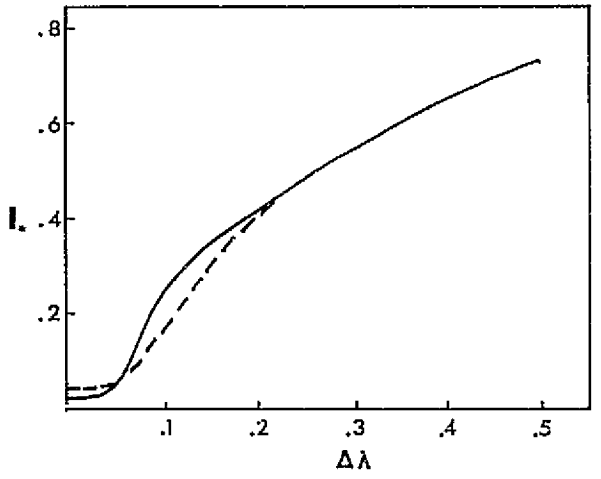

Fig. 2. Observed (dashed) and computed (solid) profiles of Na I λ5890., where I_* is the ratio of line to continuum intensity, at disk center.

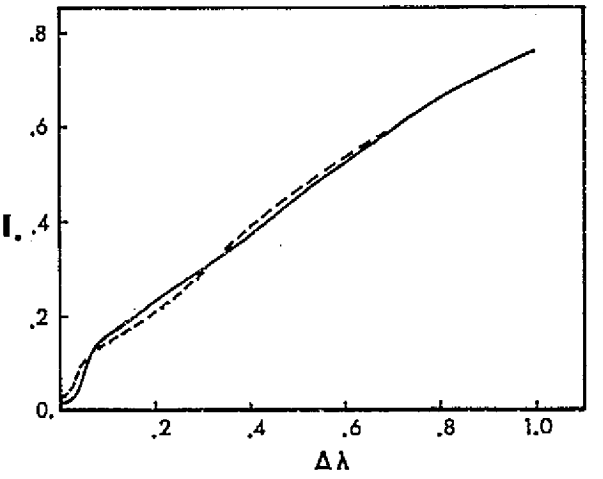

Fig. 3. Observed (dashed) and computed (solid) profiles of Ca I λ4227., where I_* is the ratio of line to continuum intensity, at disk center.

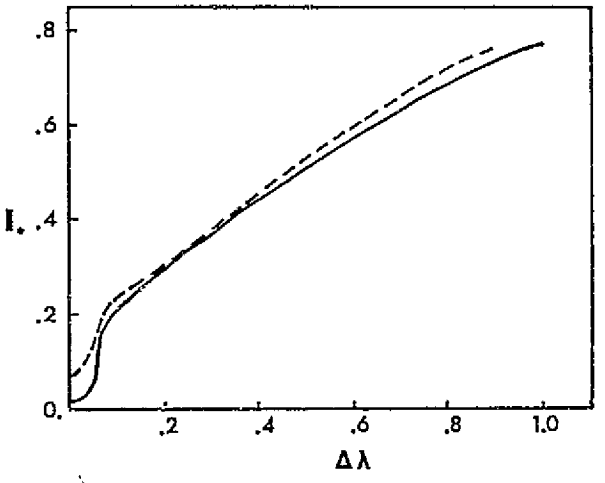

Fig. 4. Observed (dashed) and computed (solid) profiles of Mg I λ5172., where I_* is the ratio of line to continuum intensity, at disk center.

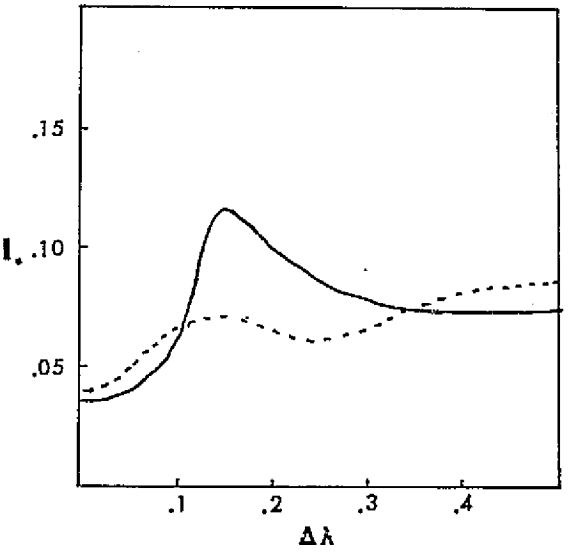

Fig. 5. Observed (dashed) and computed (solid) profiles of Ca II λ3933., where I_* is the ratio of line to continuum intensity, at disk center.

Figure 6 displays the results for the λ8542 transition of Ca II. This line is not expected to show strong coherency effects. The Doppler core is in good agreement with observation, but the wing is too bright. This may be due to the collisional broadening parameters we have used.

We compare in Figure 7 our calculated Mg II λ2795 profile to the computed profile obtained by Milkey and Mihalas (1974) in the complete redistribution case. Comparision with observations is, as with Ca II K, poor but the comparison does provide a consistency check. The differences between the two calculations are small, and are due mainly to the choice of a microturbulence model. Again, as with Ca II, partial redistribution effects may be important for the Mg II h and k lines.

The transitions we have calculated in detail represent a wide range in core formation heights and wavelength. The results of this study provide a background for calculations which account explicitly for the inhomogeneous structure of the chromosphere. The resulting two component chromosphere will then be restrained by this grid of line profiles.

VI. Acknowledgments

The authors wish to thank Dr. R. W. Milkey for helpful discussions. The assistance of the N.M.S.U. Computer Center staff is gratefully acknowledged. This work was supported by NSF Grant No. LP-43815.

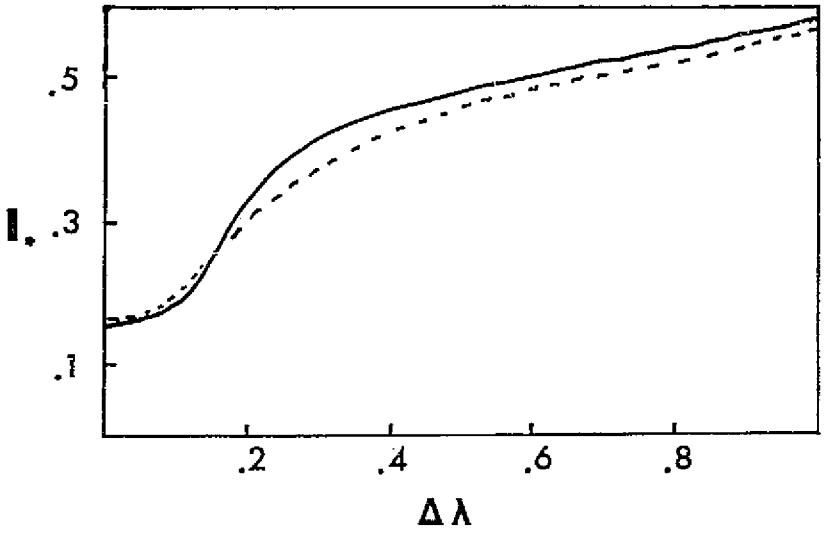

Fig. 6. Observed (dashed) and computed (solid) profiles of Ca II λ8542., where I_* is the ratio of line to continuum intensity, at disk center.

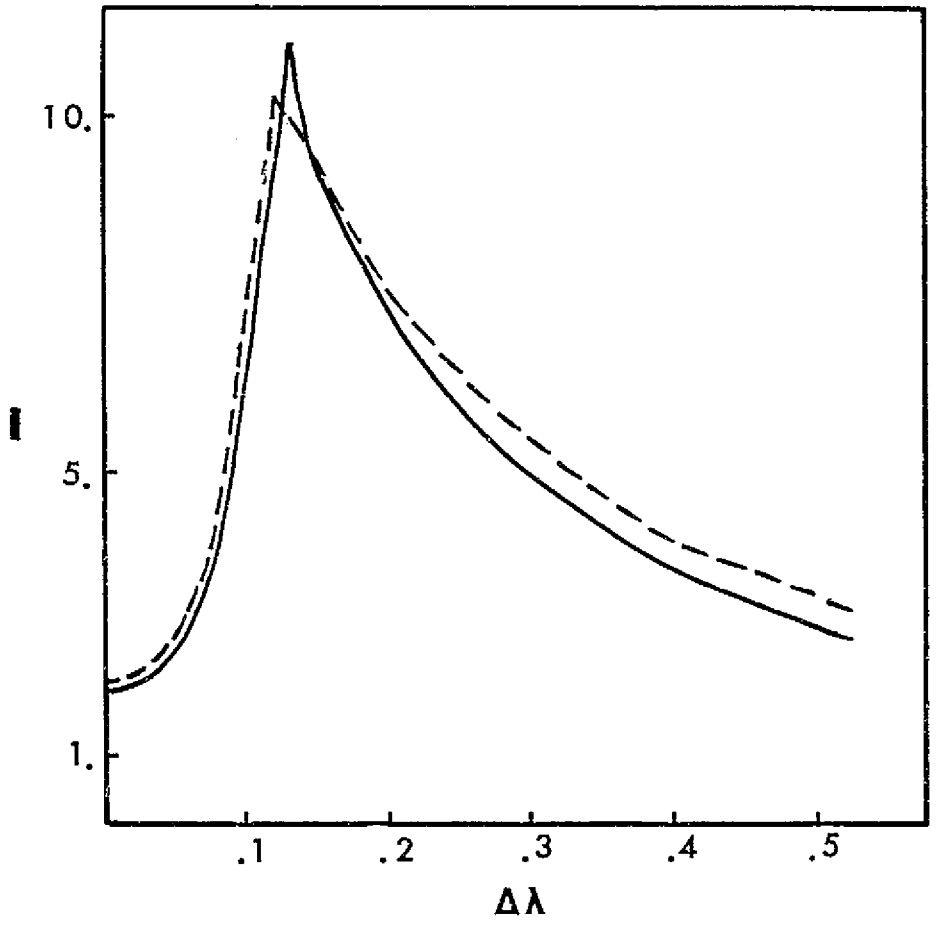

Fig. 7. The results of Milkey and Mihalas (1974) with complete redistribution (dashed) and the profile computed in this study (solid) for Mg II λ2852., where I is intensity × 10^7 in ergs/cm^2/sec/ster/Hz at disk center.

References

Allen, C. W. 1973, Astrophysical Quantities (London : Athlone).

Altrock, R. C. and Canfield, R. C. 1974, Ap. J., 173, 681.

Athay, R. G. and Canfield, R. C. 1969, Ap. J., 156, 695.

Athay, R. G. and Skumanich, 1967, Ann. Astrophys., 30, 669.

Auer, L. H., Heasley, J. N. and Milkey, R. W. 1972, KPNO Contribution No. 555.

Beebe, H. A. 1971, Solar Physics, 17, 304.

Brault, J. and Testerman, L. 1972, Kitt Peak Solar Atlas 2942-10014 Å (Preliminary Edition), (Tucson: Kitt Peak National Observatory).

Crandall, D. H., Dunn, G. H., Gallagher, A., Hummer, D. G., Kunasz, C. V., Leep, D. and Taylor, P. O. 1974, Ap. J., 191, 789.

Dumont, S. 1967, Ann. D'Ap., 30, 861.

Gingerich, O., Noyes, R. W., Kalkofen, W. and Cuny, Y. 1971, Solar Physics, 18, 387.

Lambert, D. L. and Warner, B. 1968, M.N.R.A.S., 138, 181.

Linsky, J. L. and Avrett, E. H. 1970, P.A.S.P., 82, 169.

Lites, B. W. 1973, Solar Physics, 32, 283.

Milkey, R. W. and Mihalas, D. 1974, Ap. J., 192, 769.

Shine, R. A., Milkey, R. W. and Mihalas, D. 1974, preprint.

Unno, W. 1959, Ap. J., 129, 388.

Van Regemorter, H. 1962, Ap. J., 136, 906

Weideman, V. 1955, Zs. Fur Astrophys., 101, 136.

Weise, W. L., Smith, M. W. and Miles, B. M. 1969, Atomic Transition Probabilities, NSRDS-NBS-22.

EMISSIVITIES AND DETECTABILITY OF THE PURE ROTATIONAL TRANSITIONS OF MOLECULAR HYDROGEN

TIMOTHY J. SCHNEEBERGER

Department of Astronomy, New Mexico State University, Las Cruces

Abstract

The emissivities of the infrared rotational transitions of H_2 are calculated for temperatures from 10 °K to 6000 °K. The calculations are made for several ratios, R, of Para (J=0) to Ortho (J=1) H_2. The possibility of detecting these transitions in interstellar molecular clouds is discussed.

Subject headings: infrared - interstellar matter - spectra, molecular

I. Introduction

Molecular hydrogen was first detected in the interstellar medium by Carruthers (1970) with rocket UV observations of the resonant Lyman band. Subsequent UV observations by Smith (1973) and Spitzer et. al. (1973) qualitatively confirm the theory of Hollenbach, Werner, and Salpeter (1971), who predicted an increasing abundance of H_2 with increasing optical depth in interstellar clouds. This prediction is also supported by the work of Garzoli and Varsavsky (1966) and Meszaros (1968), who have shown that, in areas of large visual absorption, the column density of atomic hydrogen is constant or decreases with increasing visual absorption. This is interpreted as the result of increasing H_2 formation. Meszaros (1968) concludes that 50% of the material in a dark cloud near ρ Oph may be molecular hydrogen.

Appreciable densities of H_2 have also been inferred from observations of molecular emission in interstellar clouds. Heiles (1968) found that H_2 number densities up to $570/cm^3$ were needed to explain the normal OH emission in several dark clouds (see table 3). Penzias et. al. (1972) find that H_2 number densities of $10^3/cm^3$ may be expected in dark clouds. Penzias et. al. (1971) have pointed out the importance of H_2 in the formation of molecules with observed radio emission.

Thus, although H_2 does not appear to be present in significant amounts in the general interstellar medium, it is likely to be a major constituent of cool clouds. Detection of H_2 in such clouds then provides a valuable probe in interpreting the nature of the galactic molecular clouds. The strong interstellar absorption in the UV limits the usefulness of the resonant electronic transitions of H_2. Varsavsky (1966) suggested that the infrared, (2μ), vibration - rotation transitions from the first excited vibrational level might be detectable; however, no clear evidence of these transitions in molecular clouds has yet been made (Gull and Hartwit 1971). The low excitation temperatures of the pure rotational transitions make them likely candidates for detection in cool clouds. Despite the low transition probabilities and atmospheric absorption due to H_2O and CO_2, we show that several of these transitions should be detectable with available equipment. To determine which transitions are detectable we calculate the emissivity of the transitions at temperatures appropriate to molecular clouds, and in addition, we must estimate the H_2 density, temperature, size, and distance of several molecular clouds.

II. Emissivity Calculations

Table 1 gives the Einstein transition probabilities, adopted from Aannestad (1973), the wavelengths, and J values of the transitions

included in these calculations. Para and ortho (triplet) transitions are included up to the J = 15 rotational level. We assume that collisions dominate since the radiative transition probabilities are small. We also assume no mixing of para and ortho states. Para to ortho radiative transitions are forbidden, and Spitzer et al. (1973) point out that collisional para to ortho transitions are rare.

We may then write the Boltzmann equation,

$$n(J)/n(JJ) = (g(J)/g(JJ)) \exp(-h\Delta\nu(J\rightarrow JJ)/KT),$$

where:

$g(J) = 2J+1$, para states

$g(J) = 3(2J+1)$, ortho states

$JJ = J-2$.

See Herzberg (1950) for a discussion of the statistical weights. We reduce all number density ratios to the appropriate ground state, n(J,para)/n(0) and n(J,ortho)/n(1). We normalize to the total H_2 density by writing $1 = \sum_J n(J)$. By choosing a ratio of para to ortho H_2, $R = n(0)/n(1)$, we may solve for the individual n(J's) and calculate the emissivity by:

$$EM(J\rightarrow JJ) = n(J)\, h\Delta\nu\, (J\rightarrow JJ)\, A(J\rightarrow JJ)$$

where:

$n(J)$ = the number density per H_2 molecule in level J

$\Delta\nu(J\rightarrow JJ)$ = the transition frequency

$A(J\rightarrow JJ)$ = the Einstein probability in sec^{-1}

$EM(J\rightarrow JJ)$ = the emissivity in ergs/sec/H_2.

Such calculations have been made by Bussoletti (1973) for para states only, and by Dalgarno and Wright (1972) who choose the thermal equilibrium value for R, R = 1/3. However Spitzer et al. (1973) found R = 1 in the

Table 1

Transition Parameters

Transition J→JJ	Wavelength Microns	Einstein A sec^{-1}
2-0	28.2174	$2.9x10^{-11}$
3-1	17.0345	$4.6x10^{-10}$
4-2	12.2788	$2.6x10^{-9}$
5-3	9.6651	$9.3x10^{-9}$
6-4	8.0246	$2.4x10^{-8}$
7-5	6.9074	$5.3x10^{-8}$
8-6	6.1033	$1.0x10^{-7}$
9-7	5.5005	$1.7x10^{-7}$
10-8	5.0337	$2.7x10^{-7}$
11-9	4.6617	$4.0x10^{-7}$
12-10	4.3571	$5.6x10^{-7}$
13-11	4.1004	$7.7x10^{-7}$
14-12	3.8767	$1.0x10^{-6}$
15-13	3.6746	$1.4x10^{-6}$

Timothy J. Schneeberger

general interstellar medium in the direction of 13 stars from Copernicus results. Field et. al. (1966) discuss the uncertainty in the value of R. We have chosen to perform the calculations at several physically plausible values of R.

III. Results

Table 2 lists the cases which were chosen for discussion. The results are shown in Figures 1 through 7 for temperatures from 10 °K to 1000 °K. Calculations were also made for temperatures up to 6000 °K. H_2 may form in interstellar shock waves at these high temperatures (Field et. al 1968) but Heubner (1974) has pointed out that Boltzman statistics are unlikely to hold in these conditions.

The results for R = 1/3 at low temperatures ($T \leq 200$ °K) are in excellent agreement with those of Dalgarno and Wright (1972), small differences being due to the slightly different transition probabilities chosen. The case where $R = 1.x10^{12}$ was chosen to approach Bussoletti's (1973) assumption of pure para H_2. The results are in close agreement up to the J = 4 level, but the present results are systematically higher for the higher levels.

In the following discussion the notation (J→JJ) refers to the emissivity of the transition from the J level to the JJ level. We first consider the temperature range of 10 °K to 500 °K. For R = 1/3, the J = (3→1) transition dominates from 100 °K to 370 °K; above 370 °K the J = (4→2) and J = (5→3) transitions become larger. Below 100 °K the J = (2→0) transition is dominant. For R = 1, the J = (3→1) transition dominates from 140 °K to 250 °K. Spitzer et. al. (1973) found H_2 rotational temperatures between 150 °K and 200 °K. If such temperatures exist in molecular clouds we may expect the 17μ transition to be more easily

detectable than the 28 μ transition, for the values of R discussed above. We can see that the emissivity is a strong function of temperature so that detection of two transitions would provide valuable temperature information.

Higher values of R, R = 500 and R = 1×10^{12}, may occur if the J = 0 ground state is favored at formation of the molecule, or if the temperature is low (20 °K) for a sufficient period of time after formation. In these cases we can see the suppression of the ortho transitions with the J = (2→0), (4→2), and (6→4) transitions being the only significant ones.

From 500 °K to 1000 °K the ortho transitions J = (5→3) and J = (7→5) dominate for R = 1/3. At the remaining values of R the para transitions J = (4→2) and J = (6→4) dominate. From 1000 °K to 6000 °K all the upper levels become populated and the J = (2→0) and J = (3→1) transitions are orders of magnitude below the higher transitions due to the increasing population of the upper levels and the low transition probabilities of the two transitions to the ground state.

IV. Detectability

Table 3 lists seven molecular clouds for which H_2 densities, temperatures, sizes and distances have been estimated. Objects 3 through 7 are from Heiles (1968), and use is made of the nomenclature used therein. The temperatures for objects 3 through 7 were taken as one half of the upper limit to the spin temperature found by Heiles (1968). Data for Sgr A and Sgr B2 are taken from Bussoletti (1973). We consider transitions detectable if a flux of 1×10^{-10} ergs/cm^{2}sec is incident at the top of the atmosphere. This is a reasonable value for moderate to large telescopes even if a total transmission of only 1% is found since

Table 2

Parameters of the Emissivity Calculations

R	Temperature	Figure
1/3	10 - 500 °K	1
1	10 - 500 °K	2
500	10 - 500 °K	3
$1x10^{12}$	10 - 500 °K	4
1/3	500 - 1000 °K	5
1	500 - 1000 °K	6
$1x10^{12}$	500 - 1000 °K	7

Table 3

Parameters of Molecular Clouds

No.	Object	1950 RA	Dec	T°K	Dist (pc)	Radius (pc)	H_2/cm^3
1	Sgr A	18^h15^m	-27°	30	10^4	7.5	10^5
2	Sgr B2	18 14	-28	150	10^4	.75	10^6
3	1-1D	22 36	+75	150	500	1.5	220
4	1F	22 15	+73	150	400	.5	510
5	2	4 38	+25	170	113	7.8	42
6	4	16 24	-24	130	77	.55	570
7	L134	15 51	- 4	50	170	4.7	73

Nos. 1 and 2 from Bussoletti (1973)

Nos. 3 through 7 from Heiles (1968)

the noise equivalent power of present infrared detectors is in the neighborhood of 10^{-14} watts (Low 1961). If sufficient resolution is obtainable we find that at least four of these clouds can be detected. Tables 4 through 6 give the expected flux for different values of R.

The calculations for temperatures up to 6000 °K which may occur in interstellar shock waves are not presented here since Non-LTE effects are likely to be significant under these conditions. However, we may point out that even in the most favorable conditions (Mach 20 collision with no magnetic field), the emission from H_2 formed in these regions is not detectable with available equipment (see Field et. al. 1968).

V. Conclusions

We have presented emissivity calculations for a range of para to ortho ratios and have shown that several molecular clouds not previously considered may be detectable. We have pointed out the strength of the 17μ transition at low temperatures and low values of R. It must be emphasized that these calculations are strongly dependent on the temperature chosen for the molecular clouds. This fact, along with the strong dependence of other observed interstellar molecules on the presence of H_2, underlies the importance of detecting H_2 in the galactic molecular clouds.

This work was completed with the support of an N.S.F. Traineeship, and computations were done at the NMSU Computer Center. I thank Drs. R. F. Beebe and W. Heubner for their comments on this paper.

Table 4

Expected Flux (ergs/cm^{2}sec), R = 1/3

Object	Transition	Flux
Sgr B2	2-0	3.52×10^{-10}
	3-1	1.39×10^{-9}
1-1D	2-0	2.48×10^{-10}
	3-1	9.79×10^{-10}
	4-2	3.66×10^{-10}
1F	3-1	1.32×10^{-10}
2	2-0	2.14×10^{-9}
	3-1	1.08×10^{-8}
	4-2	7.96×10^{-10}
4	2-0	8.06×10^{-10}
	3-1	2.31×10^{-9}

Table 5

Expected Flux (ergs/cm^{2}sec), R = 1

Object	Transition	Flux
Sgr B2	2-0	6.81×10^{-10}
	3-1	8.97×10^{-10}
	4-2	1.02×10^{-10}
1-1D	2-0	4.77×10^{-10}
	3-1	6.31×10^{-10}
2	2-0	4.00×10^{-9}
	3-1	6.84×10^{-9}
	4-2	1.51×10^{-9}

Table 6

Expected Flux (ergs/cm^{2}sec), R = 1×10^{12}

Object	Transition	Flux
Sgr B2	2-0	1.27×10^{-9}
	4-2	1.91×10^{-10}
1-1D	2-0	8.94×10^{-10}
	4-2	1.34×10^{-10}
1F	2-0	1.20×10^{-10}
2	2-0	7.27×10^{-9}
	4-2	2.73×10^{-9}

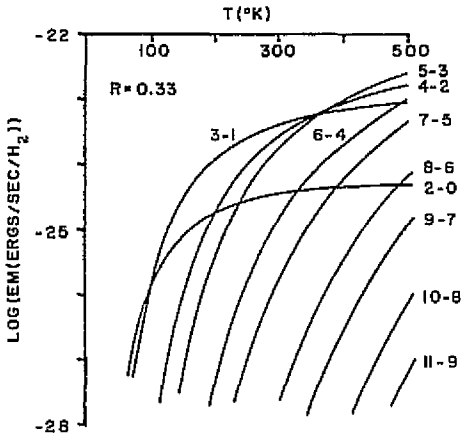

Fig. 1. -- The emissivity of molecular hydrogen at low temperatures with R = 1/3. The rotational transitions are labelled in the sense, JJ-J. Note the strength of the 3-1 transition.

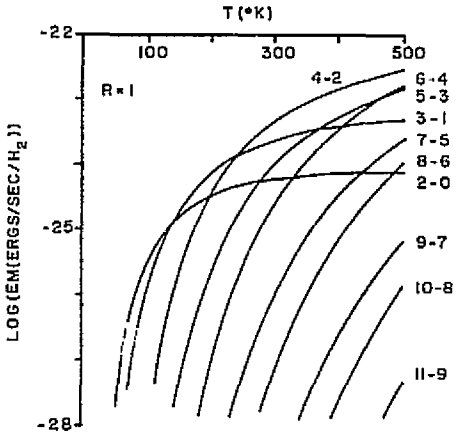

Fig. 2. -- The emissivity of molecular hydrogen at low temperatures with R = 1.

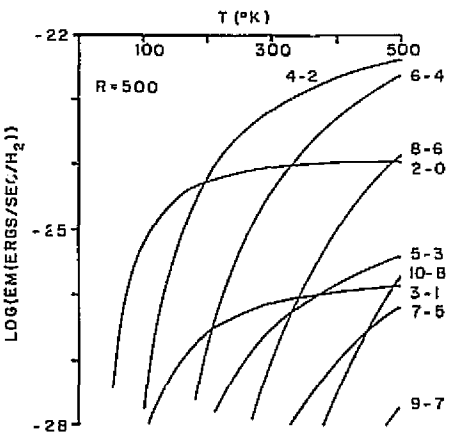

Fig. 3. -- The emissivity of molecular hydrogen at low temperatures with R = 500.

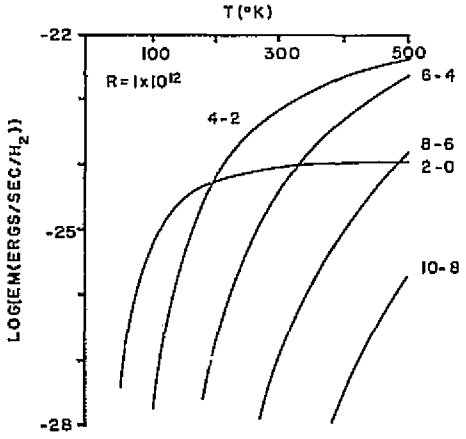

Fig. 4. -- The emissivity of molecular hydrogen at low temperatures with R = 1. x 10^{12}.

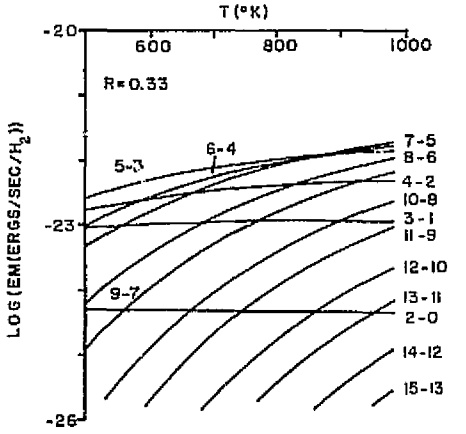

Fig. 5. -- The emissivity of molecular hydrogen for temperatures greater than 500 °K, with R = 1/3.

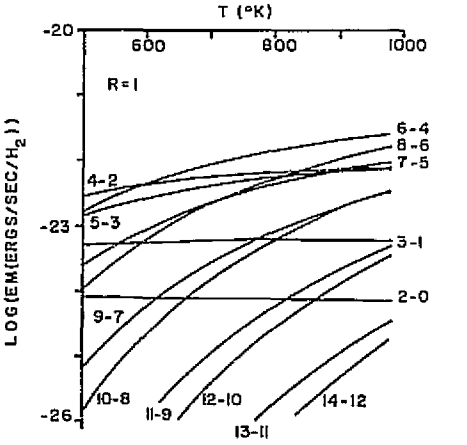

Fig. 6. -- The emissivity of molecular hydrogen for temperatures greater than 500 °K, with R = 1.

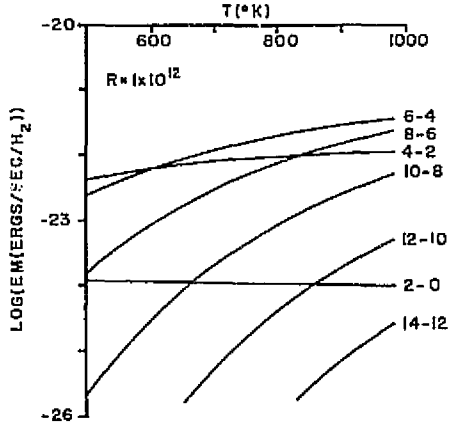

Fig. 7. -- The emissivity of molecular hydrogen for temperatures greater than 500 °K, with R = 1. x 10^{12}.

REFERENCES

Aannestad, P. 1973, Ap. J. Suppl. 25, 205.

Bussoletti, E. 1973, Astron. Astrophys. 23, 125.

Carruthers, G. 1970, Ap. J. 161, L81.

Dalgarno, A., Wright, E. L. 1972, Ap. J. 174, L49.

Field, G., Rather, J., Aannestad, P., Orszag, S. 1968, Ap. J. 151, 953.

Field, G., Somerville, W., Dressler, K. 1966, Ann. Rev. Ast. Astrophys. 4, 207.

Garzoli, S., Varsavsky, C. 1966, Ap. J. 145, 79.

Gull, T., Hartwit, M. 1971, Ap. J. 168, 15.

Heiles, C. 1968, Ap. J. 151, 919.

Herzberg, G. 1950, Spectra of Diatomic Molecules, New York: Van Nostrand, 133-134.

Heubner, W. 1974, private communication.

Hollenbach, D., Werner, M.W., Salpeter, E. E. 1971, Ap. J. 163, 165.

Low, F. 1961, J. Op. Soc. Am 51, 1300.

Meszaros, P. 1968, Astrophys. Space Sci. 2, 210.

Penzias, A., Solomon, P., Jefferts, K., Wilson, R. 1972, Ap. J. 174, L43.

Penzias, A., Solomon, P., Wilson, R., Jefferts, K. 1971, Ap. J. 168, L53.

Smith, A. 1973, Ap. J. 179, 11.

Spitzer, L., Drake, J. F., Jenkins, E. B., Morton, D. C., Rogerson, J. B., York, D. G. 1973, Ap. J. 181, L116.

Varsavsky, C. 1966, Space Sci. Rev. 5, 419.

PHOTOMETRY OF R CORONAE BOREALIS

DENNIS W. DAWSON

and

EDWARD F. TEDESCO

Department of Astronomy, New Mexico State University

ABSTRACT

Visual and photoelectric observations of R Coronae Borealis are presented, including a number of observations surrounding the 1974 minimum. The recent visual history of the variable is examined and the discrete cloud obscuration model is considered.

INTRODUCTION

R Coronae Borealis is the prototype of a group of stars that exhibits relatively brief, but large, drops in brightness that may be superimposed on much slower variations in the level of peak brightness. Other stars in the group include ρ Cas, UV Cas and SU Tau. However, R CrB has received the most attention because of its brightness and, recently, because of the discovery of an infrared excess (Stein et al. 1969). The infrared spectrum of R CrB indicates that the star is embedded in what are probably graphite grains.

Spectra and photometry of R CrB at its normal maximum brightness ($V \cong 5.8$) are consistent with an F8 Ib supergiant with about $0^m.06$ interstellar reddening. Fernie et al. (1971) found evidence for low-amplitude pulsations ($\Delta V \sim 0^m.15$) with a period of 44 days; assuming a Cepheid-type period-mass-radius relation, they derived $M \cong 2\ M_\odot$, $R \cong 100\ R_\odot$, and $M_V = -5.5$. Assuming that the level of peak brightness for R CrB represents freedom from circumstellar reddening, the intrinsic colors are B-V = 0.53 and U-B = 0.01.

I. BRIGHTNESS OF R CORONAE BOREALIS, 1966-1975

Photoelectric and visual magnitude estimates were obtained from various sources in the literature, specifically Forrest et al. (1971, 1972), Fernie et al. (1971), and various individual observations reported in the IAU Circulars. The authors obtained photoelectric photometry at the Blue Mesa and Tortugas Mountain sites during the 1974-75

observing season; some of these observations have been published elsewhere (Dawson and Tedesco 1974, Dawson 1974, Tedesco and Dawson 1974). The visual (V) light curve of R CrB is shown in Figure 1; the 1974 minimum is shown in more detail in Figure 2.

Fernie et.al. (1971) discussed the prolonged suppression of the level of maximum light (between 1963 and 1968) in terms of a large, slowly-expanding shell of carbon particles, citing as evidence the slow drop in B-V between 1966 and 1967 in contrast to its virtual constancy throughout the 1966 minimum. Figure 1 indicates that the dissipation of this general veiling was not really complete until late 1970; some of the infrared results obtained during this period (for example, Forrest et.al. 1971) may have to be modified because of the presence of this shell.

Figure 2 shows that the 1974 minimum was very asymmetric with the drop in light much steeper than the subsequent rise; this is consistent with the picture of a cloud being formed in the line of sight. Minimum light for R CrB occurred between JD 2442083 and JD 2442088 (Feb. 4 and Feb. 9); no photometry was available between these dates.

II. PHOTOMETRY FOLLOWING THE 1974 MINIMUM

UBV photometry obtained during rising light is given in Table I. A discordance between visual and photoelectric brightnesses near maximum light was noted, leading us to examine the four brightest comparison stars on the AAVSO "b" chart. Our results are listed in Table II and show that the two brightest stars (SAO 084005 and 084053) are, respectively, 0.24 and 0.21 magnitude fainter than their chart values. All visual estimates brighter

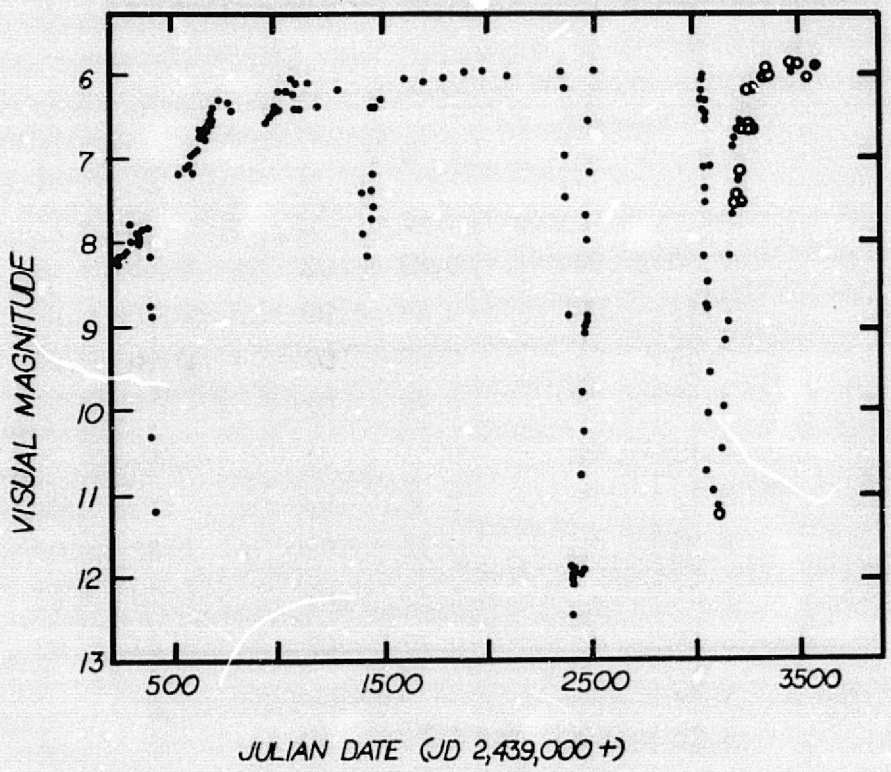

Fig. 1 -- Visual magnitude variations of R Coronae Borealis during the period 1966-1975. Filled circles represent visual estimates, while open circles are photoelectric determinations.

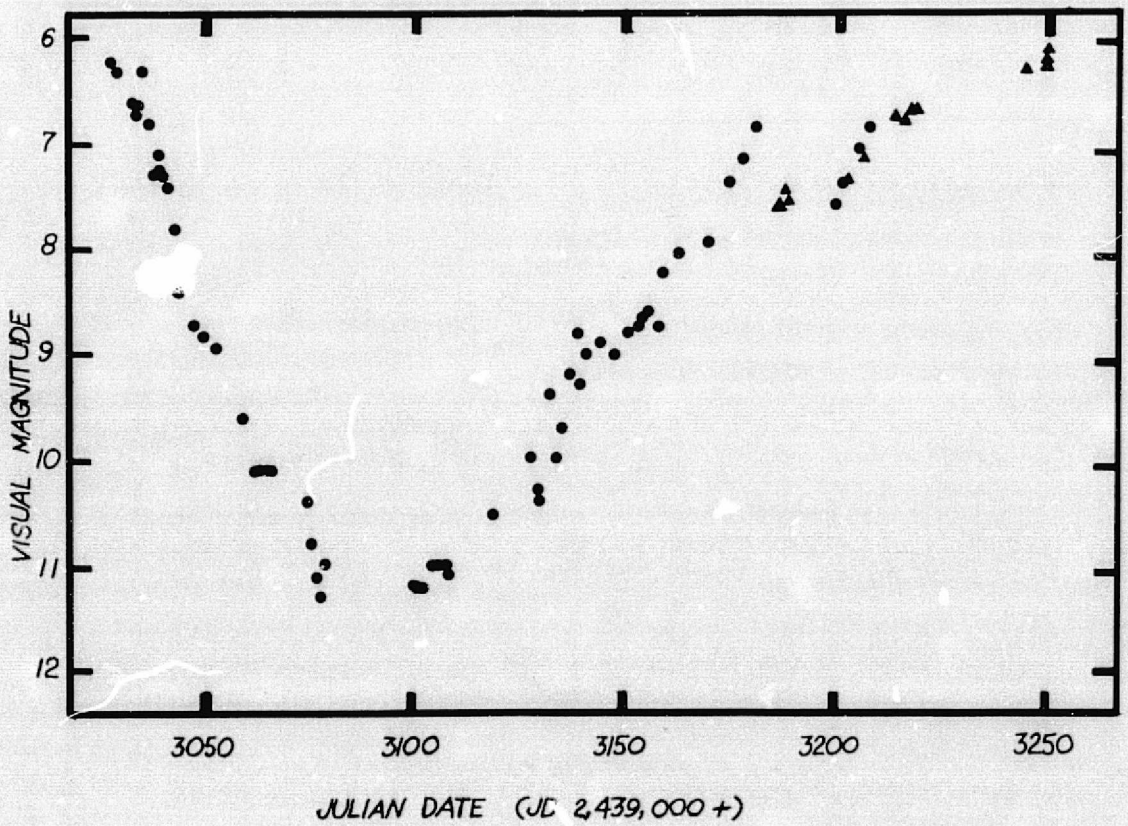

Fig. 2 -- Detail of the 1974 minimum. Triangles represent photoelectric determinations by the authors, circles visual observations.

TABLE I

Photoelectric Observations of R CrB 1974-75

UT Date	V	B-V	U-B	Telescope[a]
May 20.258	7.60 ± .04	0.83 ± .03	0.32 ± .02	B
May 21.226	7.45 .03	0.83 .02	0.32 .03	B
May 22.303	7.56 .05	0.85 .02	0.29 .03	B
June 5.243	7.36 .07	0.78 .02		T
June 9.192	7.13 .06	0.86 .01		T
June 17.168	6.73 .05	0.81 .03		T
June 19.208	6.78 .02	0.77 .02	0.32 .03	B
June 20.253	6.71 .03	0.76 .03	0.34 .03	B
June 21.255	6.69 .02	0.76 .02	0.34 .03	B
July 17.155	6.28 .05			T
July 22.3	6.20 .03	0.78 .02		T
Oct. 2.139	6.03 .02	0.65 .02	0.23 .08	B
Oct. 3.079	6.03 .01	0.61 .02	0.16 .02	B
Oct. 5.084	5.98 .03	0.64 .02	0.22 .02	B
Feb. 13.469	5.86 .04	0.59 .04		B
Mar. 2.394	5.93 .02	0.47 .02	0.18 .03	B

[a]B = Blue Mesa 61 cm reflector; T = Tortugas 41 cm reflector

TABLE II

Observations of AAVSO Comparison Stars

SAO Number	V	B-V	U-B	Telescope[a]	Number of nights observed
084005	7.44 ± .02	0.47 ± .03	-0.01 ± .03	B,T	5
083985	8.05 .03	0.60 .02		T	1
084053	7.81 .05	1.20 .02		T	4
084057	8.32 .03	1.08 .02		T	1

[a]B = Blue Mesa 61 cm reflector; T = Tortugas 41 cm reflector

than $8^m.5$ were corrected by adding $0^m.2$; this, as can be seen from Figure 2, results in better agreement between the visual and photoelectric observations.

III. DISCUSSION

Much of the non-periodic behavior of R CrB can be explained by assuming that the spatial distribution of carbon particles is not uniform; in particular, a model involving discrete, optically thick clouds can be used to explain the lack of a distinct anticorrelation of visual and infrared brightnesses that might be expected if the visual energy were absorbed by the grains and reradiated at longer wavelengths (Forrest et.al. 1972). It is more difficult to explain the suppression of the level of maximum in such a model unless a large, dissipating cloud were spreading across the line of sight.

If the discrete cloud model is valid for members of the R Coronae Borealis group, it will be difficult to predict future minima; continued monitoring of these variables is therefore important. The short-term pulsations of R CrB should also be studied in an effort to interpret the graphite grain replenishment mechanism.

REFERENCES

Dawson, D. W. 1974, IAU Circular No. 2689.

Dawson, D. W. and Tedesco, E. F. 1974, IAU Circular No. 2678.

Fernie, J. D., Sherwood, V., and du Puy, P. L. 1972, Ap. J., 172, 383.

Forrest, W. J., Gillett, F. C. and Stein, W. A. 1971, Ap. J. (Letters), 170, L29.

Ibid., 1972, 178, L1.

Stein, W. A., Gaustad, J. E., Gillett, F. C. and Knache, R. F. 1969, Ap. J. (Letters), 155, L3.

Tedesco, E. F. and Dawson, D. W. 1974, IAU Circular No. 2717.

INTERMEDIATE-BAND PHOTOMETRY OF FAINT STANDARD STARS

Dennis W. Dawson
Department of Astronomy
New Mexico State University

ABSTRACT

Preliminary values of color indices in the DDO photometric system are presented for sixteen stars of $V \geq 5$, as an extension of faint standards lists.

INTRODUCTION

The David Dunlap Observatory system uses six intermediate-band filters whose central wavelengths were chosen to cover important features in the spectrum of a late-type star. Calibrations of the color indices with physical parameters, by Janes (1972) and Osborn (1971), allow one to estimate T_{eff}, log g, [Fe/H], M_V and reddening directly from the photometry.

Although a number of standards lists exist (for example, McClure and Van den Bergh 1968, Janes 1972 and McClure 1974), only a small fraction of the stars is fainter than V=6. It is desirable to add to the numbers of faint standards.

This work presents results of photometry of sixteen stars obtained during a program of variable-star photometry at Blue Mesa Observatory extending from April, 1974 through October, 1975.

THE OBSERVATIONS

I used the abbreviated system, filter set "NMSU" as described by Janes (1974), and an ultraviolet filter similar to that of Osborn. A 23 arc-second aperture and EMI 9502-B photocell (S-11 surface, cooled) were also used in the photometry.

Extinction coefficients for the color indices are low, near the level of observational errors, because of the small central wavelength separations; the use of mean extinction coefficients is adequate. I have adopted values from Kitt Peak (Janes 1971) for the abbreviated system and derived a value for the index C3841 by an extrapolation of the wavelength dependence of extinction (Figure 3, Hardie 1962); these values are: k[C4548]=0.051, k[C4245]=0.056, k[C4142]=0.023, k[C3841]=0.055.

Nightly reductions use an average of thirteen standards (11-28). In computing the average colors, I weighted each nightly value by $[1/\sigma]$ so that nights with high transformation errors received proportionately low weights.

Table I lists the program stars by HD or BD numbers, or by their designations in the articles where finder charts are available. Following the name are a visual magnitude, the source of the V photometry or the finder chart, the color indices and their standard errors, and the number of measures used to form the indices.

These colors are to be regarded as provisional and the last digit taken at low weight. Color residuals were improved by a cleaning of the filters in October, 1975.

Photometry on these and other faint stars is continuing and will be reported in a forthcoming edition of the Publications.

REFERENCES

Hardie, R.H. 1962, in Astronomical Techniques, W. A. Hiltner, ed. (Chicago: U. of Chicago Press).

Janes, K.A. 1971, private communication. 1972, Ph.D. thesis, Yale University. 1974, Astrophys. J., 189, 423.

McClure, R.D. 1974, private communication.

McClure, R.D. and Bergh, S. van den 1968, Astron. J., 73, 313.

Osborn, W.H. 1971, Ph.D. thesis, Yale University,

Table I. Results of Photometry

Star Ident.	V	Source	C4548	σ	C4245	σ	C4142	σ	C3841	σ	n
φ Cas	5.00	P1	1.081	011	0.479	.014	0.048	.007			3
BD -9°2086	6.57	PKSW	1.375	.009	1.366	.024	0.225	.023	-0.020	.017	4
HD 116817	6.98	DD	1.225	.016	0.809	.024	0.153	.026	-0.537	.024	6
HD 10494	7.32	DD	1.243	.017	0.628	.018	0.112	..019			5
BD +60°2532	8.31	P2	1.193	.024	0.686	.015	0.130	.020	-0.580	.016	4*
BD +25°0734	8.60	DD	0.995	.005	0.561	.004	0.012	.006	-0.914	.015	3
BD +25°4301	8.80	DD	1.197	.011	0.890	.007	0.205	.012	-0.526	.012	2
BD +21°3451	8.81	DD	1.257	.001	0.902	.001	0.270	.007	-0.439	.007	2
BD +2°0521	8.83	DD	1.007	.020	0.568	.005	0.044	.017	-0.875	.024	4
BD +3°0453	9.20	DD	0.781	.024	0.342	.015	0.043	.006	-0.924	.025	3
CT Ori comp.	9.36	DP	0.764	.022	0.279	.007	0.023	.014	-1.137	.031	3*
EI Peg comp.	9.92	DP	1.020	.006	0.615	.024	0.055	.005	-0.750	.014	3
DF Cyg comp.	10.21	PKSW	0.980	.020	0.564	.028	0.033	.020	-0.828	.028	3
TW Cam comp.	11.25	DP	1.063	.024	0.632	.015	0.005	.016	-0.816	.030	4
V360 Cyg comp.	11.33	PKSW	0.969	.002	0.558	.018	0.062	.033	-0.843	.035	3
EQ Cas comp.	11.47	PKSW	1.305	.011	0.979	.025	0.140	.012	-0.382	.001	3

* For these objects, C3841 is based on only one measure but it is included for completeness. The error of the color transformation for the night is given.

Source Key

DD — V photometry by the author
P1 — P.Pesch 1959, Astrophysical Journal, 130, 764
P2 — P.Pesch 1960, ibid. , 132, 689
DP — D.L. DuPuy 1973, ibid. , 185, 597
PKSW — G.W.Preston,W.Krzeminski,J.Smak and J.A.Williams 1963, ibid., 137, 401

SEYFERT GALAXIES--A STUDY OF BRIGHTNESS VARIATION AND STELLAR CONCENTRATION

Dennis W. Dawson
Department of Astronomy
New Mexico State University

ABSTRACT

UBV photometry of Seyfert galaxies is analyzed for variations in nuclear magnitude. Using multiple apertures permits one also to estimate the stellar concentration; four Seyfert and two normal spiral galaxies are compared.

INTRODUCTION

A galaxy may be regarded as a member of the Seyfert group when it displays: 1) a bright compact nuclear region; 2) broad emission lines from permitted and forbidden transitions; 3) nuclear continuum emission; 4) multiple velocity systems of absorption lines; 5) a large nuclear ultraviolet excess; and/or 6) time variation of the nuclear brightness, particularly in the level of the UV continuum.

Although Pacholcyzk (1971) has identified a possible five-year variation for NGC 4151, Seyfert galaxies do not, in general, exhibit any regular changes in brightness. Outbursts occur on a scale of weeks (for example, MacPherson 1972), and fluctuations in the UV continuum strength appear to be their source.

OBSERVATIONS

UBV photometry of the Seyfert galaxies NGC 4051, 4151, 6814 and 1068, and of the normal galaxies NGC 7331 and 224, was taken at the Blue Mesa site between May and December, 1974. I used a cooled EMI 9502 B photocell, a Teledyne 4701 voltage-to-frequency converter, and five diaphragms subtending 123, 91, 63, 32 and 23 arc-seconds.

Each galaxy was optically centered in the largest aperture, but I corrected its position in the smaller ones when necessary, the twenty-three arc-second aperture appeared to be the smallest that I could use and still obtain a reasonable repetition of counts in a given filter; excursion effects became noticeable for smaller diaphragms.

Every count for a particular filter was the mean of at least three ten-second integrations. The faintest Seyfert studied, NGC 6814, had six or more integrations per filter.

Use of an average of fifteen secondary UBV standards per night insured an adequate reduction of the data; mean transformation errors (σ) were $0^m.018$ in B-V, $0^m.024$ in U-B, and less than $0^m.03$ in V. Standards were taken from the list of Iriarte et. al. (1965).

Table 1 lists the program objects, dates observed, aperture ratio (to be defined), and the UBV magnitudes. The results of similar photometry by Zasov and Lyutyi (1973) show good agreement with the present data.

Table 1

The Observations

Galaxy	Date	X	V	B	U
NGC 4051	19 May 1974	.49	11.30	11.98	11.92
		.36	11.65	12.34	12.30
		.20	12.12	12.87	12.86
		-.10	12.82	13.58	13.63
		-.24	13.10	13.87	13.96:
NGC 4151	22 May 1974	.64	11.02	11.70	11.26
		.51	11.20	11.85	11.37
		.35	11.36	12.00	11.48
		.05	11.66	12.25	11.59
		-.09	11.84	12.36	11.65
	18 June 1974	.64	10.92	11.55	11.08
		.51	11.09	11.64	11.14
		.35	11.24	11.76	11.20
		.05	11.51	11.95	11.26
		-.09	11.62	12.01	11.29
NGC 6814	21 June 1974	.75	11.64	12.48	12.91
		.62	11.80	12.70	12.89
		.46	12.26	13.18	13.37
		.16	13.12	14.15:	14.54:
	17 October 1974	.75	10.88	12.01	12.29
		.62	11.27	12.17	12.41
		.46	11.63	12.55	12.84
		.16	12.81	13.50	13.78
NGC 1068	17 October 1974	.40	9.14	9.90	10.01
		.27	9.27	10.00	10.10
		.11	9.49	10.23	10.32
		-.19	9.90	10.70	10.81
		-.33	10.15	10.98	11.19
NGC 7331	16 October 1974	.29		11.57	
		.16		11.73	
		.00		12.04	
		-.30		12.66	
		-.44		13.04	
NGC 224		-.91		8.39	
		-1.04		8.80	
		-1.20		9.36	
		-1.50		10.49	
		-1.64		11.05	

Table 2

Coefficients of the Quadratic Fits

Galaxy	α	$\alpha\beta$	B(0)	Type
NGC 4151*	-0.26	0.63	12.13	Sab
NGC 1068	0.84	1.55	10.38	Sb
NGC 7331	0.99	1.86	12.02	Sb
NGC 224	0.68	1.91	6.08	Sb
NGC 4051	-0.96	2.36	13.36	Sbc
NGC 6814*	1.98	4.51	14.50	Sbc

* Mean of two nights

MULTIPLE APERTURE PHOTOMETRY

Diaphragm sizes are scaled to a galaxy's angular extent by use of the APERTURE RATIO, X, and a value of the face-on diameter, D(0), tabulated in De Vaucouleurs (1964); specifically, $X=\log A - \log D(0)$ where A and D(0) are in arc-seconds.

Let B(X) be the integrated magnitude within an aperture that scales to X for the particular galaxy. De Vaucouleurs (1964) found that B(X) may be expressed as a quadratic function of X for ordinary galaxies, viz.

$$B(X) = B(0) - \alpha X(\beta - X)$$

If the stellar populations outside the nucleus are the same for a Seyfert and an ordinary galaxy of similar development, the brightness functions will differ in a predictable fashion. Treating the quasi-stellar nucleus of a Seyfert galaxy as a point source of magnitude B_n leads to an intensity at X=0 of

$$I'(0) = 10^{-0.4B(0)} + 10^{-0.4B_n}$$

and a composite brightness function (disk plus core) of

$$B'(X) = -2.5 \log I'(0) - \alpha X(\beta - X)$$

Now suppose the nuclear magnitude and the magnitude B(0) differ by a constant, κ. The composite brightness function may be written

$$B'(X,\kappa) = -2.5 \log \left[10^{-0.4B(0)} + 10^{-0.4(B(0)+\kappa)}\right] - \alpha X(\beta - X)$$

B(0) values are tabulated in De Vaucouleurs (1964). One compares the observed data [B'(X)] with curves of $B'(X,\kappa)$ for various κ, and the value giving the best fit leads to the nuclear magnitude: $B_n = B(0) + \kappa$.

A quantity of interest in examining the similarity of the extranuclear stellar populations is the concentration parameter $\Delta B(X)$ defined by Zasov and Lyutyi (1973):

$$\Delta B(X) = B(-1) - B(X)$$

This quantity should be free from effects caused by an abnormal nucleus and relate directly to the population outside it.

STELLAR CONCENTRATIONS

I assumed a quadratic brightness law could be used to describe the brightness functions of Seyfert as well as ordinary galaxies and formed $\Delta B(X)$ for all the program objects. The quadratic assumption allows an extrapolation to X=-1, which is necessary since none of the apertures used was small enough to measure B(-1) directly. If $[\alpha,-\alpha\beta,B(0)]$ are the fit coefficients it follows that

$$B(-1) = \alpha + \alpha\beta + B(0)$$

Table Two lists the coefficients of the quadratic fits for the program galaxies, and those with $\Delta B < 5$ are shown in Figure One with a de Vaucouleurs empirical relation for early-type galaxies.

Figure One indicates that NGC 4151 tends to have a steeper brightness gradient than an ordinary early-type galaxy. Both NGC 4051 and NGC 6814 display little central concentration while NGC 1068 appears to have a nearly ordinary extranuclear population.

Zasov and Lyutyi (1973) found that except for NGC 4051 (6814 was not studied) most Seyfert galaxies have $1.5<n<2$ for a brightness power law $I_b(r)=1/r^n$, in contrast to $0.8<n<1.4$ for ordinary galaxies. NGC 4051 has $n=0.5$, and the current data indicate a similar brightness law for NGC 6814.

The "quasi-observable" quantity $\Delta B(0) = \alpha(1+\beta)$ can be related to the values of the radial brightness exponent n. Figure Two, which combines the present data with that of Zasov and Lyutyi, shows this relation which has the rough linear form $n \sim 3 - 3/4\ \Delta B(0)$. It is difficult to argue whether the steeper brightness gradients of the more active Seyfert galaxies are prerequisites for the Seyfert behavior or are the result of it. The gradient does diminish with Hubble type, as shown by the concentrations of NGC 4151 (Sab), NGC 1068 (Sb) and NGC 4051 (Sbc) and the lack of Seyfert activity in Sc galaxies. This is also shown by the correlation of $\alpha\beta$ with Hubble type as shown in Table Two.

TIME VARIATIONS OF BRIGHTNESS

The galaxies NGC 4151 and NGC 6814 were examined on two different occasions, and both had varied significantly in brightness and color. The brightness functions are shown in Figures Three and Four.

Note the large ultraviolet excess of NGC 4151. As U-B changed little but B-V changed by roughly $0^m.15$, we must assume that the brightness changes occurred at nearly equal levels in U and B but much less in V; this is consistent with a change in the level of the ultraviolet continuum.

NGC 6814 displays a brightness change that suggests equal rise in V and B rather than in U. However, the galaxy was faint enough in U that the U-B colors are open to some question. The work of MacPherson (1972) confirms the constancy of B-V for this galaxy.

Variations in the U filter amount to $0^m.36$ for NGC 4151 and $0^m.77$, for NGC 6814.

DISCUSSION

Photometry of the four Seyfert and two ordinary galaxies has shown that differences exist between them, not only in the nucleus but also in the stellar population outside it. The concentration of this population appears correlated with activity.

Two of the Seyfert galaxies showed time variation of brightness, consistent with previous results in the literature.

REFERENCES

Iriarte, B., Johnson, H. L., Mitchell, R. I. and Wisniewski, W. K. 1965, Sky and Telescope, 30, 21.

MacPherson, G. J. 1972, Pub. Astron. Soc. Pacific, 84, 392.

Pacholczyk, A. G. 1971, Astrophys. J., 163, 449.

Vaucouleurs, G. de 1964, Reference Catalog of Bright Galaxies (Univ. of Texas Press).

Zasov, A. V. and Lyutyi, V. M. 1973, Soviet Astronomy-AJ, 17, 169.

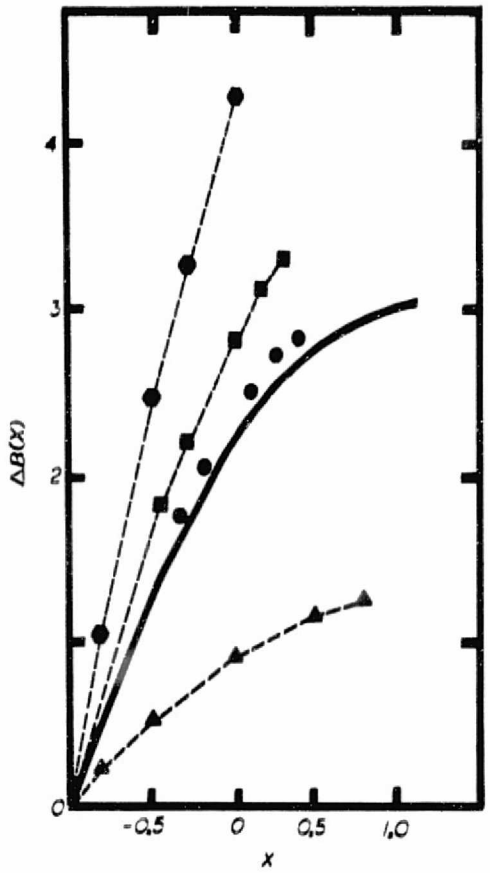

Fig. 1-Concentration parameter ΔB as a function of aperture ratio for the program galaxies. The solid line represents the de Vaucouleurs empirical relation for early-type galaxies. Symbols used: hexagons, NGC 4061; squares, ordinary Sb spiral NGC 7331; circles, NGC 7068; triangles, NGC 4151.

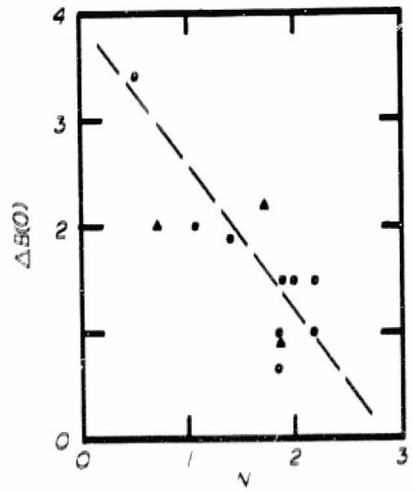

Fig. 2-Relation between ΔB(0), obtainable from the quadratic brightness-law fit, and the exponent n of the radial brightness variation. Circles, data of Zasov and Lyutyi; triangles, this study.

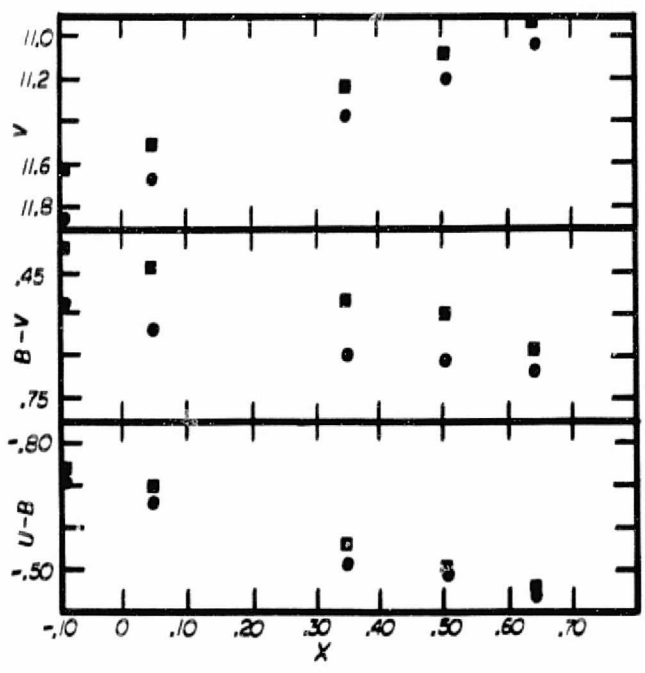

Fig. 3-Magnitude and color variation for NGC 4151. Circles, observations of May 22, 1974; squares, observations of June 18, 1974.

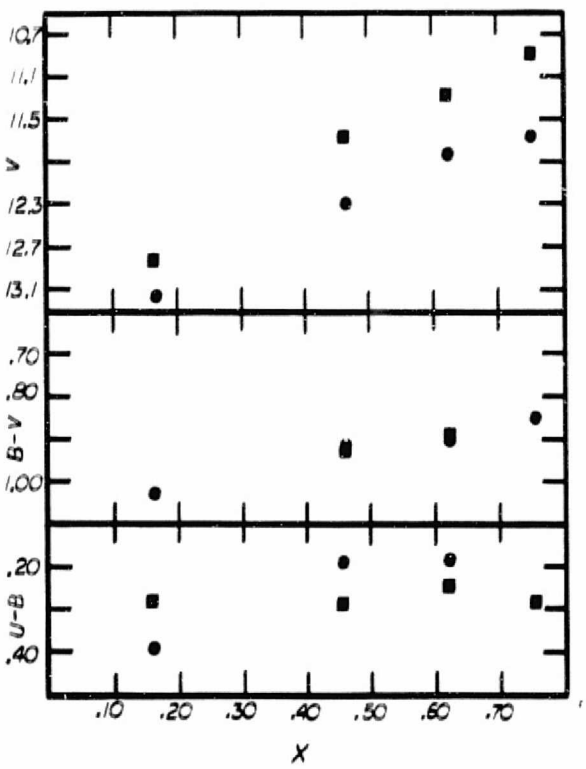

Fig. 4-Magnitude and color variation for NGC 6814. Circles, observations of June 21, 1974; squares, observations of October 17, 1974.

TESTING OF A PHOTOELECTRIC PHOTOMETER

I. Determination of Operational Parameters

Dennis W. Dawson and Edward F. Tedesco
Department of Astronomy
New Mexico State University

ABSTRACT

Observations over four months are used to evaluate magnitude and color transformations, extinction coefficients and a gain table for the photoelectric photometer of the 41 cm. reflector at the Tortugas Mountain site. We discuss ways of increasing the efficiency and accuracy of this system.

INTRODUCTION

To obtain consistent and accurate results from a photoelectric system it must be calibrated against some standard photometry such as the UBV system, which now has an extensive list of secondary standard stars.

The 41 cm. Rhodes reflector (f/34 at the time of this study, subsequently altered to f/12) is equipped with a photometer designed by Dr. James Cuffey, which uses an RCA 1P21 photomultiplier tube and dry-ice cooling (optional). Cooling was not employed in the present work.

Also in the system are: 1) a set of standard UBV filters, plus red-leak and dark; 2) a radium star for gain calibration; 3) eighteen half-magnitude gain steps, labeled A-G and 0-10 by increasing sensitivity; and 4) four apertures subtending 20, 30, 40, and 60 arc-seconds. The filter and aperture options are controlled at the telescope; a sliding prism sends incident light through a viewing eyepiece or onto the photocathode. A Mosely Model 680 strip chart recorder is used.

We used the 60 arc-second aperture for the calibration. A carbon star (19 Psc) produced negligible red leak deflections in all filters. The amplifier was zeroed by adjusting the voltage to produce minimum drift at the recorder as the gain steps were traversed, and the recorder was then manually zeroed at gain A. The photocell was run routinely at 870 volts.

CALIBRATION PROCEDURE

We observed forty-two bright stars in the Arizona-Tonantzintla (Iriarte et.al., 1965) from October, 1973 through February, 1974 to obtain color and gain calibrations; observations made in June, 1974 augmented the extinction data obtained earlier. We took deflections at various hour angles and at a number of different gain steps; signals above 32% full scale were considered usable (the figure was established by examining the maximum tolerable errors in the final transformations).

Most of the stars observed near the meridian lie between the celestial equator and zenith; we assumed the extinction of a unit air mass for stars within one hour of the meridian so that color transformations could be obtained in terms of a zenith color value. This procedure is entirely adequate for general transformations; extinction corrections will be discussed in the last section.

COLOR TRANSFORMATIONS

Transformations of the observed meridian (B-V) and (U-B) colors to the standard system were first obtained by the procedure outlined above; enough stars were available to allow U,B,V deflections on the same gain (or any two on the same gain) , and a gain calibration was not needed at this point. The majority of stars used actually lay within 1/2 hour of the meridian.

The best fits to the data are:

$$(B-V)_{std} = 1.17\ (B-V) + 0.89 \quad (\pm 0^m.01) \quad n=21$$

$$(U-B)_{std} = 0.99\ (U-B) - 1.70 \quad (\pm 0^m.07) \quad n=12$$

The (B-V) transformation is accurate enough to be used directly, if desired, since the largest error in the fit is only $0^m.04$ (see Figure 1). The (U-B) data have more scatter because of fewer points and the generally lower signal through the U filter; the two largest deviations at one end suggest the importance of a (B-V) color term.

THE GAIN CALIBRATION

Stars and the radium source were used for gain calibration on several occasions. Comparison of nightly results was generally poor, but we finally attributed this to using data at deflections too low for adequate reading accuracy. We therefore reworked the gain calibration using high deflection data only and adopted this as the correct one (it is listed in Table I); its accuracy was tested by taking readings for one star at two different gains and reducing them to an arbitrary gain with the table. The magnitudes thus obtained were normally within $0^m.03$ of each other.

We also tested the gain calibration on stars at 0h, ±2.5h and ±5h hour angle to determine whether tube magnetization had affected the original results. No such effects were found.

MAGNITUDE CALIBRATIONS

UBV deflections at various gains were reduced to an arbitrary gain with the gain table and then related to the Arizona magnitudes. We chose gain 0 as the arbitrary gain since it was used most often during the work.

The REDUCED MAGNITUDE (the magnitude in a given filter in terms of its value at gain 0) is defined so that

$$m_r = -2.5 \log D_f \ \pm \sum_{i=1}^{n} \Delta m_i$$

where n is the number of gain steps above zero (plus sign) or below zero (gains A-G, minus sign), and D_f is the deflection at the given gain in filter f.

Linear least-squares fits of the reduced and Arizona magnitudes, shown in Figure 2, yield the following transformations:

$$V_{std} = 0.995\ V_r + 7.54 \quad (\pm 0^m.05)$$

$$B_{std} = 0.964\ B_r + 8.21 \quad (\pm 0^m.11)$$

$$U_{std} = 1.006\ U_r + 6.59 \quad (\pm 0^m.08)$$

The fits are reasonably tight though uncorrected for extinction, mean errors being $0^m.05$, $0^m.07$ and $0^m.04$ respectively. The small scatter in V reflects the accuracy of the gain calibration, while the larger B,U scatter may result from the larger extinction through these filters.

The colors derived from this independent approach agree fairly well with those of Figure 1, especially in the U-B color. The (B-V) transformations differ, but the B magnitude calibration has a large scatter; we therefore feel that use of the first (B-V) calibration will lead to more consistent results.

EXTINCTION CORRECTIONS

Some scatter in the previous results is due to lack of an explicit correction for extinction.

To determine extinction coefficients, a number of program stars (red-blue pairs) were observed nightly over many hour angles. A program written by one of us (E.Tedesco) computed magnitudes, sec Z and air mass using the sec Z polynomial of Bemporad (see Hardie, 1965). We also took extinction measures at the Rhodes telescope during June, 1974 and at the Blue Mesa 61 cm. telescope during four nights in May, 1974 , to supplement this data. Table II lists the coefficients so obtained; weights were assigned on the basis of internal consistency and the number of measurements taken per star per night.

There is excellent agreement among the different determinations. We have adopted the weighted mean values $k_v = 0.150$, $k_{b-v} = 0.112$ and $k_{u-b} = 0.215$ magnitude/air mass.

Applying the "correction" term -k(X-1) to the observed meridian colors (assumed to be zenith values) leads to an estimate of the effect of including extinction on the color transformations. That is, the true zenith (X=1) colors are derived using the extinction explicitly and this determination is compared with the uncorrected transformation for tightness of fit. Using fifteen of the stars in the original (B-V) transformation, we derive the following transformation coefficients, correlations, and average and standard deviations:

$$(B-V)_{std} = 1.184(B-V)_{corr} + 0.899 \quad r=99.98\% \quad AD=0^m.009 \quad SD=0^m.011 \quad \text{EXPLICIT CORRECTION}$$

$$(B-V)_{std} = 1.185(B-V) + 0.883 \quad r=99.97\% \quad AD=0^m.010 \quad SD=0^m.013 \quad \text{NO CORRECTION}$$

Neglecting differential extinction near the meridian has little effect on the color transformation.

Table I
Gain Calibration

GAIN STEP	RATIO	MAGNITUDE DIFFERENCE
B/A	1.595	0.507
C/B	1.608	.516
D/C	1.642	.538
E/D	1.685	.566
F/E	1.563	.485
G/F	1.778	.625
0/G	1.540	.469
1/0	1.672	.558
2/1	1.820	.650
3/2	1.743	.603
4/3	1.598	.509
5/4	1.597	.508
6/5	1.672	.558
7/6	1.589	.503
8/7	1.515	.451
9/8	2.000	.753
10/9	3.800	1.449

Table II
Mean Extinction Coefficients

UT Dates	K_v	K_{b-v}	K_{u-b}	n
17-19 Nov.1973	.198	.090	.218	26
5 June 1974	.130	.100	.201	11
19-22 May 1974	.152	.127	.225	30

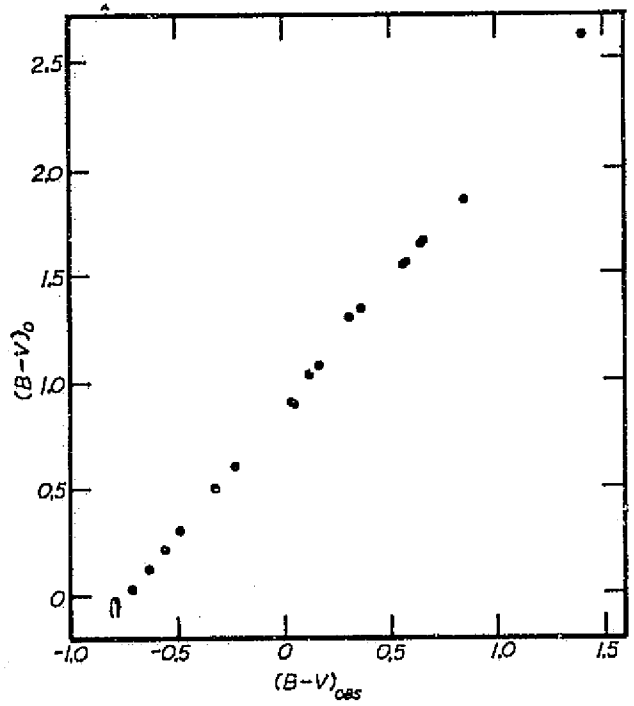

Figure 1a - Transformation of observed meridian B-V colors to the standard system.

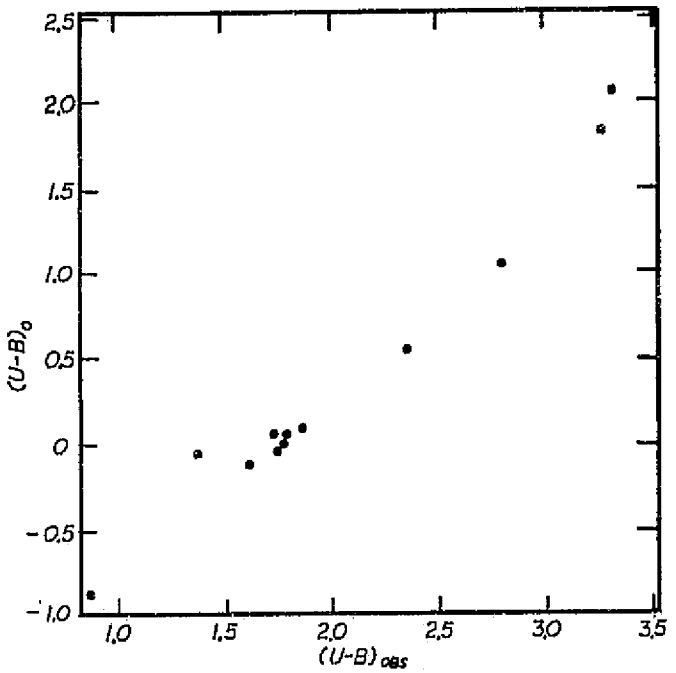

Figure 1b - Transformation of observed meridian U-B colors to the standard system.

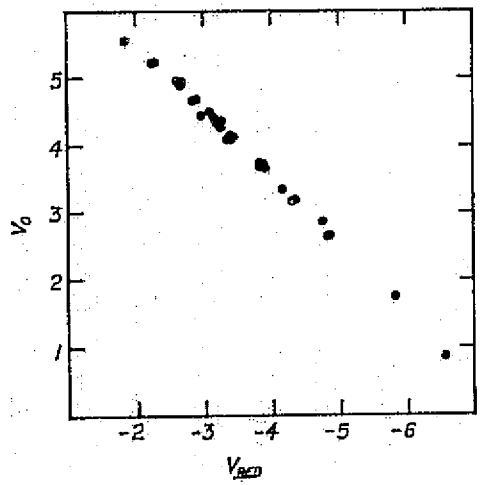

Figure 2a - Transformation of reduced V magnitudes to the standard system.

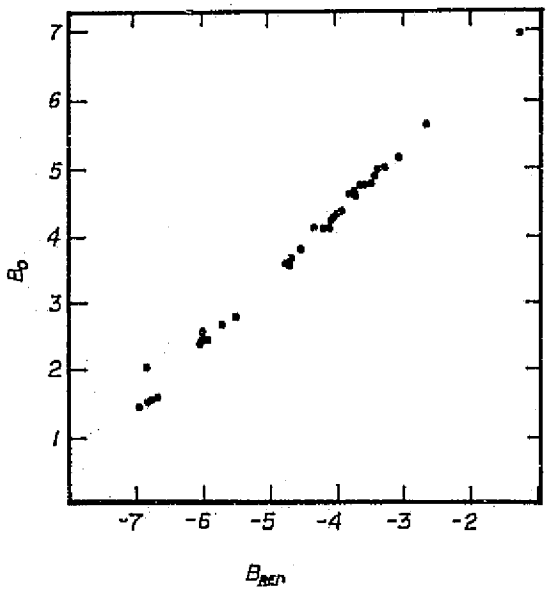

Figure 2b - Transformation of reduced B magnitudes to the standard system.

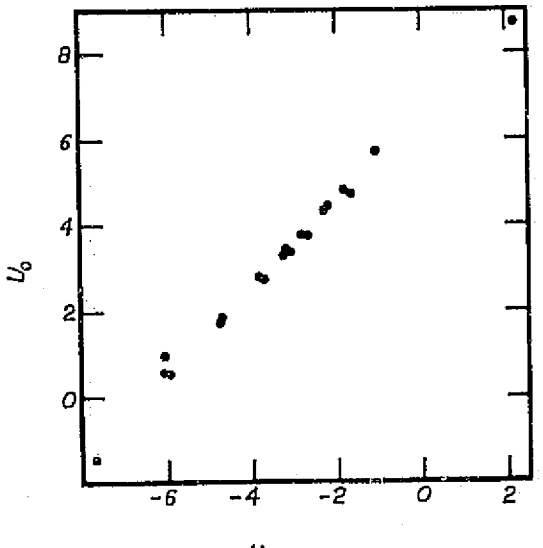

Figure 2c - Transformation of reduced U magnitudes to the standard system.

CONCLUSION

The Rhodes telescope and photometer are a stable and accurate system well-suited to observational projects. In uncooled 870-volt operation, stars of 7th magnitude gave signals larger than 32% full scale on gain 8 (gains 9 and 10 were not used as they suffer from thermal noise and non-linearity) using the f/34 configuration. Initial investigation of the f/12 system shows that 8th magnitude may be reached routinely on gain 8 (uncooled); cooling will certainly extend this limit by lowering dark noise and allowing the tube to be operated at higher voltages.

REFERENCES

Hardie, R.H. 1962, in Astronomical Techniques, W.A. Hiltner, ed. (Chicago: U. of Chicago Press), p.180

Iriarte, B., Johnson,H.L., Mitchell,R.I. and Wisniewski,W.K. 1965, Sky and Telescope, 29, 21

TESTING OF A PHOTOELECTRIC PHOTOMETER

II. Observational Testing

DENNIS W. DAWSON

and

EDWARD F. TEDESCO

Department of Astronomy, New Mexico State University

ABSTRACT

We demonstrate the versatility of the 41 cm. Tortugas reflector's photoelectric system through observations of V566 Oph and R CrB with four associated AAVSO comparison stars, these observations having been made between May and October, 1974.

INTRODUCTION

In a previous paper (Dawson and Tedesco, 1976) we evaluated the photoelectric system of the 41 cm. Tortugas reflector. The testing included forming a gain calibration and observing standard stars to obtain extinction coefficients and color transformations to the standard UBV system.

The present work explores observational uses of the system during the 1974 observing season. The photocell, operated at -870 volts, was used uncooled except for the observations of V566 Oph.

I. V566 OPHIUCHI

On July 24, 1974 we explored the capability of the Tortugas system for real-time photometry through differential photometry of the short-period W Ursae Majoris-type binary V566 Oph (P = .4096 day, m_{pg} = 7.60-8.09). Observations extended from 5^h to 8^h Universal time.

Measures of the variable alternated with those of a nearby comparison star (BD +4°3558) and sky. We used a Hewlett-Packard Model 405c digital voltmeter and paper-tape output from a Hewlett-Packard 561B digital recorder. Samples were taken every five seconds and a dozen samples averaged to yield about ±1 minute time resolution.

Results of the observations are displayed in Figure 1, which is a two-point smooth of the dozen-sample averages. The photometry indicates that V566 Oph reached maximum light at 6h45m ($\pm 2^m$) Universal time.

It is very unlikely that differential extinction could cause the observed maximum as most of the data were obtained when V566 Oph was already west of the meridian. A brightening in sky level due to the city lights of Las Cruces was noticed at 8h, but the trend in the variable data was toward fainter magnitudes.

II. R CORONAE BOREALIS

We carried out UBV photometry of R CrB at the Tortugas and Blue Mesa sites between May and October 1974, as the star emerged from a February minimum. An average of 5 standard stars was observed each night and the usual reduction techniques were applied. The color transformation errors were normally below $0^{m}.03$.

We compared the Tortugas data with determinations from Blue Mesa to test their reliability. Figure 2 shows V magnitudes from both sites: squares represent the Blue Mesa data and circles the Tortugas observations. Inter-agreement is good; there appear to be no systematic differences.

III. COMPARISON STAR MAGNITUDES

Magnitudes of several comparison stars on the AAVSO charts for R Coronae Borealis were obtained during the photometry of that variable. Initial results showed discrepancies between AAVSO magnitudes and the photoelectric values, and a more extensive investigation was begun.

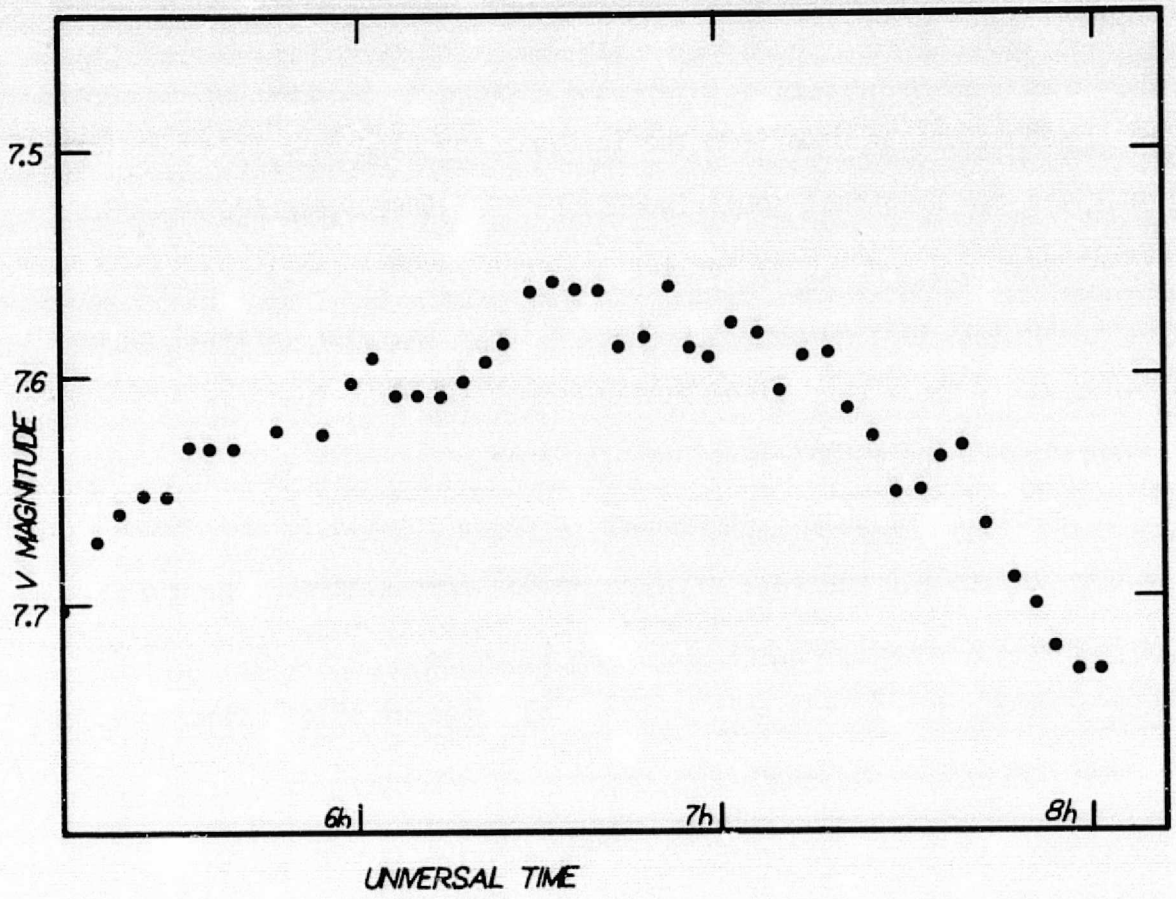

Figure 1: Lightcurve of V566 Oph on July 24, 1974. Two-point smooth of dozen sample averages.

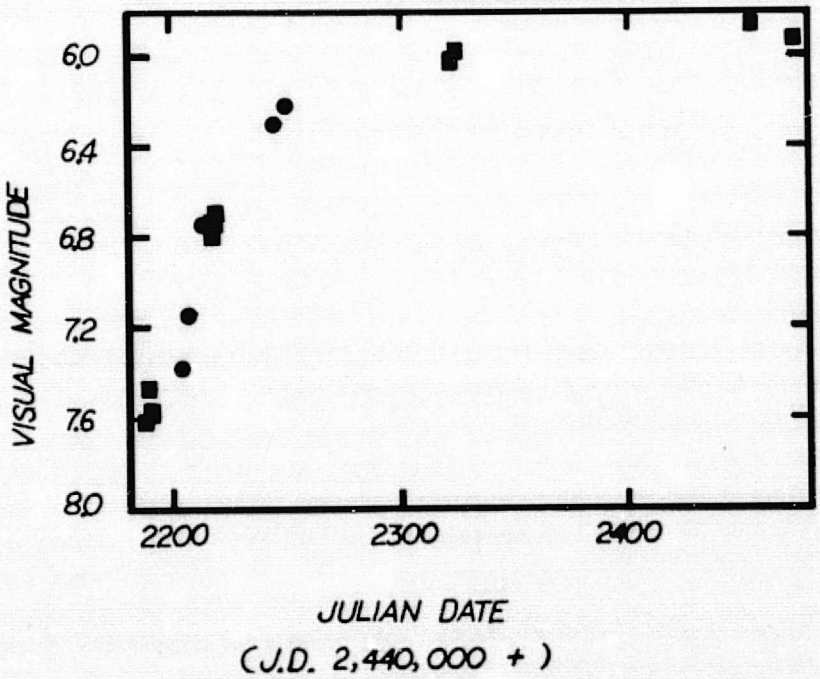

Figure 2: Blue Mesa (squares) and Tortugas (circles) observations of R CrB.

Reductions of data from the Tortugas and Blue Mesa sites indicate that the two brightest comparison stars (SAO 084005 and SAO 084053, magnitudes 7.2 and 7.6 respectively on the AAVSO charts) are actually $0^m.24$ and $0^m.21$ fainter than the chart values; therefore, visual observations using these comparison stars (when R CrB is bright) will tend to overestimate the magnitude of the variable.

An effect of this sort appears in comparing visual and photoelectric data for the 1974 minimum; it was corrected by adding $0^m.2$ to all visual observations brighter than V = 8.5. The corrected light curve shows better agreement between the types of observation.

IV. CONCLUSION

The projects outlined above demonstrate that the Tortugas photoelectric system is well-suited to work on objects of intermediate brightness. Accessibility of the facility and ease of operation make it ideal for instructional and patrol work.

ACKNOWLEDGMENT

We wish to thank Mr. Gary Cowart for technical advice and assistance in the observations of V566 Oph.

REFERENCE

Dawson, D. W. and Tedesco, E. F. 1976. In preparation, this journal.

PHOTOMETRIC CALIBRATION OF PLANETARY PHOTOGRAPHS

Reta F. Beebe

Department of Astronomy

New Mexico State University, Las Cruces, New Mexico

This article summarizes the basic data and approach for calibrating photographic plates obtained with the 61-cm telescope at the Tortugas Mountain Station of New Mexico State University Observatory. Since this is the fundamental calibration of our planetary data it is of use to all in-house users as well as other individuals who use our data.

BASIC CALIBRATION

All photographic plates taken at the 61-cm telescope at the Tortugas Mountain Station are calibrated by imprinting a sensitometric strip on them. The printer, constructed at the Lowell Observatory in 1967, utilizes a rapidly rotating sector wheel to produce the exposure steps in the calibration strip. The sector wheel contains a slotted pattern in the outer twenty percent of its radius, arranged so that at a given radius the number of slots and their angular extent determine the time-averaged illumination for a given step in the wedge. The pattern, which repeats itself every 180° rotation of the wheel, has been chosen so that the exposures increase in steps of $\sqrt{2}$ as the radius increases, ending with the darkest step suffering no intermittency.

The sector wheel is illuminated by a quartz-iodide lamp, and a combination of variable slit jaws and time exposures are utilized to obtain the correct exposure for a specific plate-filter combination. The filter is inserted into the light path between the sector wheel and the plate, and eleven rectangular steps are exposed along one end of the plate (see Figure 1). This approach takes advantage of the geometric properties of the sector wheel to assure repeatability of the calibration from plate to plate. Table 1 contains the calibrated values for $\log_{10}$ of the exposure for each step in the calibration strip.

TABLE 1

Calibrated values for the Sensitometric Strip

Step	$\log_{10} E$
1	0.0000
2	-0.1480
3	-0.2999
4	-0.4514
5	-0.6027
6	-0.7500
7	-0.9031
8	-1.0511
9	-1.2088
10	-1.3528
11	-1.5089

A possible disadvantage of this technique is the presence of intermittency effects. In this case, the sector wheel rotates at 3600 rpm with each step receiving at least two flashes per rotation. This yields at least 120 flashes per second. Since all our exposures

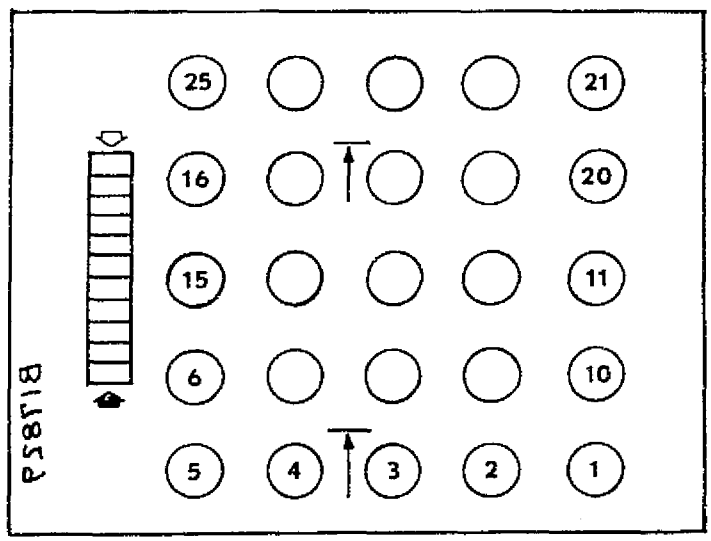

Fig. 1. A schematic of a standard 3 1/4" by 4 1/4" plate. With the emulsion side down the sensitometric strip is located on the left of the plate with the darkest step indicated by the black arrow and the lightest by the open arrow. Fiducial lines registered on the plate by the camera for geometric calibration are indicated by the thin arrows. The numbers indicate the sequence for photographing the planetary images.

are for more than one second, intermittency effects should be minimized due to the fact that the number of flashes far exceeds the number of photons absorbed by any single grain, thus the grain will not detect any non-randomness in the arrival of photons.

A standard developing technique using vertical plate hangers and the nitrogen burst technique results in a relatively homogeneous plate background; hence, any selected image on the 3 1/4 by 4 1/4 plate may be calibrated by simultaneously scanning the image and strip and applying the following procedure.

TRANSMISSION-TO-INTENSITY CONVERSION

The conversion of transmission (T) or density ($D = -\log_{10} T$) to relative intensity is accomplished in a two-step procedure. First, the scanned image is searched to ascertain that the values lie within the range of the strip and the maximum and minimum densities or transmissions are determined. Once these values are established, average densities or transmissions of those steps on the calibration strip which bracket the maximum and minimum values and the average plate background are obtained. In the case where the image is more heavily exposed than the densest step in the calibration strip, the densest step is used and the image is truncated, as explained in the latter part of this section. Average values for each step are converted to transmissions and normalized so that the plate background is equal to 1.0.

The coefficients in the following relationship

$$\log I = C_0 + C_1 \log_{10} T + C_2(\log_{10} T)^2 + C_3 \log(1-T) + C_4 T^{-1} \quad , \quad (1)$$

are determined by a least-squares method. Here T is the normalized transmission of each step in the strip. The second-order term in $\log_{10} T$ was added to the expression proposed by Honeycutt and Chaldu (1970) to improve the fit near the sky background. For high-quality plates this equation yields fits to within two percent accuracy, where the accuracy is defined as

$$I(\%) = \frac{I_0 - I_C}{I_0} \times 100 \quad , \quad (2)$$

and I_0 is the observed intensity and I_C the calculated value.

In applying equation 1 to the calibration of the image, since the fourth term becomes undefined if T is greater than 1.0, the value of the intensity is automatically set to zero in this case. On the other hand, if the transmission of the data point in question is less than the darkest calibration step the intensity is set to 1.0, hence allowing no extrapolation.

This system has been utilized for the past three years by the planetary group and appears to be an adequate procedure for obtaining a calibration technique that is readily adaptable to computerized data reduction and is accurate to the limit of our photographic process.

REFERENCES

Honeycutt, R. K., and R. S. Chaldu, 1970: The Wavelength Dependence of Three Kodak Spectroscopic Emulsions. Am. Astron. Soc. Photobulletin, No. 2, 14.

CMIT

IMPROVEMENT OF THE RHODES 16-INCH TELESCOPE ON TORTUGAS MOUNTAIN

by Clyde W. Tombaugh

Department of Astronomy
New Mexico State University
Las Cruces, New Mexico

The New Mexico State University 16-inch telescope, f3.3 primary, was purchased from Mr. Wm. Rhodes of Phoenix in 1961. Originally, it was a motor-focussing f15 Gregorian, fork mounting on a mobile trailer. It was used for seeing tests at a site a few miles north of Cloudcroft, New Mexico at about 8500 feet above sea-level.

The mounting was unsatisfactory for serious research work. Considerable modification was necessary. A number of gusset plates were welded on the inside of the fork to achieve greater rigidity. Worm wheel drives were installed on the polar and declination axes, and the base of the fork was bolted to a massive concrete pier in a dome.

The immediate need was for planetary photography. The author then designed, ground, polished and figured an f34 Gregorian, which gave excellent definition. It was little used for this purpose after 1967, when NASA provided our planetary project with an excellent 24-inch, f40 and f75 Cassegrain telescope. For a number of years, the 16-inch was used on brief spectrographic, visual, polarimetric and photo-electric projects. The tube structure resembled the Hale 200-inch telescope, except that it had an 18-inch diameter solid cylinder of thin steel, 28 inches long, which was annoyingly buffeted by gusts of wind.

The favorite program consisted of photoelectric observations with Dr. James Cuffey's photometer. The 16-inch was attractive in that it could be reached in a 15-minute drive from the campus, and several graduate students

observed variable stars, variable asteroids, and occultations of Jupiter's satellites on each other.

It became apparent that two major changes were required to better adapt the instrument for photo-electric observations: (1) To shorten the equivalent focal length and focal ratio, and (2) To get rid of the "wind-catcher" section at the upper end of the tube.

The author, having become Professor of Astronomy Emeritus, had more time than others in the Department, undertook the optical and machine alterations, with the assistance of Dr. Cuffey and some of the graduate students.

The author figured a 5-inch dia Cassegrainian mirror to give an f12 ratio, fabricated a new web support system to carry the motor-focussing mechanism, on which he mounted the new secondary mirror. The upper solid section of the tube was totally removed. Fortunately, the author found a number of arc-shaped lead weights that fit perfectly on the inside lip of the tube's upper ring to re-balance the telescope. Then the optics were carefully re-collimated. Preliminary checks indicate that now the 16-inch is quite satisfactory for photo-electric observing programs. This work was completed in April 1975.

THE NASA-NMSU AUTOMATED METEOR OBSERVATORY

Gale A. Harvey
NASA Langley Research Center

James Cuffey
New Mexico State University

ABSTRACT

A new observatory for meteor research, recently completed at New Mexico State University is providing data for study of meteor heights, velocities, orbits, and meteoroid abundances. The relatively clear desert skies of New Mexico are well suited for research of this kind. The observing equipment is suitably automated to take advantage of the long periods of favorable observing weather common to the region. Equipment for the observatory and funding are provided by NASA Langley Research Center. The main observing site, construction, and observers are provided by New Mexico State University. A second observing site is located at Corralitos Station of Northwestern University's Dearborn Observatory. Four K-24 cameras, electrically operated, provide the triangulation observations, and four Maksutov f/1.3 cameras with blazed transmission grating provide spectral coverage. The patrol cameras have operated for a year and a half and approximately 6,000 frames have been exposed by 9 March 1975. Meteor trails appear on 260 of these frames. Sixty-eight trails are of meteors photographed from two locations and thus allow trajectory and orbit determinations for 34 meteors. The spectrograph installation is largely automated. Photoelectric sensors

initiate the 2-second spectrograph exposures and electrical controls open and close the observatory at preset times. The meteor spectrographs have become fully operational only recently (May 1975) and no spectra have yet been obtained.

INTRODUCTION

The NASA-Langley Research Center (LaRC) has an on-going research program in meteor physics to better determine element abundances of meteoroids, and indirectly of certain comets (Harvey 1973a, 1973b, 1974, 1975). This relates not only to a better understanding of the near-earth particulate space environment, but is also an independent source of data for study of the early evolution of the solar system (Alfven 1971). LaRC, in cooperation with the Astronomy Department at New Mexico State University (NMSU), has established and is directing the operation of a two-station direct-camera meteor patrol at NMSU. The two-station patrol is now yielding about ten two-station meteor pairs per month. The two-station patrol provides data for meteor trajectory and orbit determinations. Trajectory data is needed to determine the effects of velocity and altitude on observed spectra, and to aid in understanding meteor radiation processes. Trajectory data is also needed for photometry of the meteors. Orbit data is needed to correlate composition with parent objects, sources of origin, and dynamics within the solar system.

Meteor spectra are needed for abundance determinations and definition of the meteor plasma. A highly automated battery of spectrographs has been added to the patrol.

The purpose of this paper is to describe the LaRC-NMSU meteor observatory facilities, instrumentation, and observing procedures.

THE METEOR TRAJECTORY AND ORBIT OBSERVATORIES

At Tortugas mountain near Las Cruces, N.M., and at the Corralitos station of Northwestern University's Dearborn Observatory, four cameras of the K-24 electrically-operated, roll-film type were set up, and aligned so that their lines of sight intersect at a height of 90 km above two points on the perpendicular bisector of the line between the two stations. The elevations of the optical axes of the four cameras are $56^{\circ}.5$ above the horizon, and the azimuths, using the abbreviations T for Tortugas, C for Corralitos, N for north and S for south are:

TN	$360^{\circ}.2$	CN	$033^{\circ}.2$
TS	21 .2	CS	$180^{\circ}.2$

The coordinates of the observatory sites are:

Tortugas	Lat	32° 17' 31".46 N	Corralitos	Lat	32° 22' 51".3 N
	Long	106° 41' 50".13 W		Long	107° 02' 27" W
	Alt	1505 meters		Alt	1454 meters

The bearing line through the two stations runs along the true azimuth $106^{\circ}.712$. Their separation is 33.73 km.

The K-24 cameras located on top of the observatory on Tortugas mountain may be seen in Figure 1. The cameras are protected from the elements by the white camera covers. Cables from the cameras lead to the power supplies and control systems located inside the silo. The K-24 cameras have Kodak Aero Ektar f/2.5 lenses of 7 inches focal length, in front of which are mounted two-bladed choppers rotating at 600 rpm,

driven by Globe Industries hysteresis synchronous motors. Meteor trails are, therefore, broken twenty times per second into segments of one fortieth of a second exposure. No attempt has been made to synchronize the choppers. The cameras use Kodak 2475 roll film 5 1/2 inches wide and 56 feet long. With magazines in proper adjustment, each roll gives 116 one hour exposures. Thus, with approximately ten exposures per night, the cameras need reloading only once every ten days. A square area of sky 40° on a side appears in each frame.

The Universal Time at the end of each exposure is recorded by a Simplex time recorder, and by an Accutron watch photographed at a corner of each frame. A photoelectric sensor which scans a nominal 30° diameter area of sky centered at altitude $56^{\circ}.5$ and azimuth $360^{\circ}.2$ is also connected to a time recorder, to record more accurately the times of occurance of meteors in the fields of view of the north-looking cameras.

After a year and a half of operation (November 1973 to March 1975) the cameras have exposed 75 rolls of film, with approximately 80 frames per roll. Of the total 6,000 exposed frames, 250 have meteor trails, 68 of which form pairs suitable for the triangulation of 34 meteors. Measurement and trajectory reduction of the two-station meteor pairs have been performed at the Physical Science Laboratory at NMSU, using standard reduction routines developed for missile trajectory studies. Meteor heights and velocities thus obtained then furnish orbital elements through additional programs.

THE METEOR SPECTROGRAPHIC OBSERVATORY

Four meteor spectrographs, consisting of 6-inch aperture f/1.3 Maksutov cameras with blazed first order transmission diffraction gratings are installed at Tortugas Mountain. All transmission optical components are transparent to near-ultra violet light (> λ3100). The cameras look at the sky through a 3 foot square opening in the roof of the Tortugas silo. Three of the spectrographs are shown in Figure 2. The square roof opening has an electrically operated sliding door. Each camera's field is circular and 21° in diameter. The spectrograms have inverse dispersions of about 120 A/mm. The fields of view of the spectrographs are in the central parts of the fields covered by the K-24 patrol cameras. The optical axes of the spectrographs are aligned as follows:

Spectrograph	Azimuth	Altitude
A	345.4	56.5
B	015.0	56.5
C	198.4	56.5
D	228.0	56.5

Since the slitless spectrographs are optimized for the near-ultra violet region of the spectrum, the azimuths actually in use are corrected for the differing deviation angles of the individual gratings, which are, for cameras A and B, 9°.7, and for cameras C and D, 14°.0. Final azimuth and altitude pointings for the spectrograph cameras, allowing for the differing gratings and the spherical trigonometry involved are:

Spectrograph	Grating	Azimuth	Altitude
A	9.7°R	002.9	57°.5
B	9.7°R	032.5	57°.5
C	14.0°R	223.7	58°.5
D	14.0°R	253.3	58°.5

Photoelectric sensors using RCA 6199 photomultiplier tubes continuously monitor the areas of sky seen by each spectrograph. Ultra violet filters eliminate much of the background sky light without lessening the sensitivity to meteors. When a meteor appears, radiation from the meteor is detected by the photomultiplier tube which is used to trigger the spectrograph shutter, opening it for a two-second exposure, and recording the time. Photomultiplier tube sensitivity must be carefully adjusted for the brightness of the sky on various nights. In practice, other sources of light often trigger spurious exposures. Passage of the moon, or of clouds illuminated by the moon often cause trouble, as do lightning flashes, even those remote from the field.

A sliding door electrically controlled is used to open and close the observing aperture in the roof. A timer switch provides for automatic opening at a suitable time at the end of evening twilight. Push buttons and relays provide manual open and manual close. A second timer switch always closes the roof aperture before dawn. Thus, once the film is loaded into the spectrographs, the installation can operate itself repeatedly. In practice, however, the need to readjust the sensitivity of the photoelectric sensors to allow for changing sky brightness limits the automatic observing periods to two or three nights when the moon is in the sky, and to seven nights when the moon is inconspicuous. Obviously the possibility of unexpected rain or snow requires careful attention on the part of the operator, who may sometimes find it necessary to make hurried trips to close up the observatory. Luckily rain and snow are not often encountered in southern New Mexico.

Each spectrograph field covers 314. square degrees, or 1.5% of the visible hemisphere. The battery of four spectrographs cover 6.% of the hemisphere. Although the hourly rate for visual meteors is 6, most of these are much too faint to record as spectra. In fact, from previous operation of these spectrographs (Harvey 1971) we may expect about four spectra per month from the use of the four spectrographs. Thus, one spectrum requires approximately eight nights of continuous exposure to the sky, and hencethe observatory must be largely automated for efficient work on the part of the observer. Therefore, the observatory is programmed by electrical timer to automatically perform the following actions.

1. Open the slit at the end of twilight.
2. Turn on the high voltage to the sensors.
3. Watch for meteors.
4. Open the spectrograph shutter when a meteor appears.
5. Control the spectrograph exposure times.
6. Turn off the high voltage to the sensors.
7. Close the slit before dawn.

CONCLUDING REMARKS

Although the observatory has been in use only a limited time, it is apparent that automated operation is vital to the project. Meteor spectra should be obtained at a rate of one per camera-spectrograph per 30 nights of observing time. With four spectrographs, the rate becomes one per eight nights of observation. Thus, the ability to operate only four nights in a row automatically increases the probability of acquisition of a meteor spectrum to an even chance. Savings in film consumption,

in travel, film processing, and film searching are significant aspects of this highly automated meteor spectra patrol.

REFERENCES

Alfven, H. 1971, Science 172, 494.

Harvey, G. A. 1971, NASA TN D-6298.

Harvey, G.A. 1973a, NASA SP-319, 103.

Harvey, G.A. 1973b, Jour. Geophysical Research 78, 3913.

Harvey, G.A. 1974, Astron. Jour. 79, 333.

Harvey, G. A. 1975, Jour. Geophysical Research, to be published.

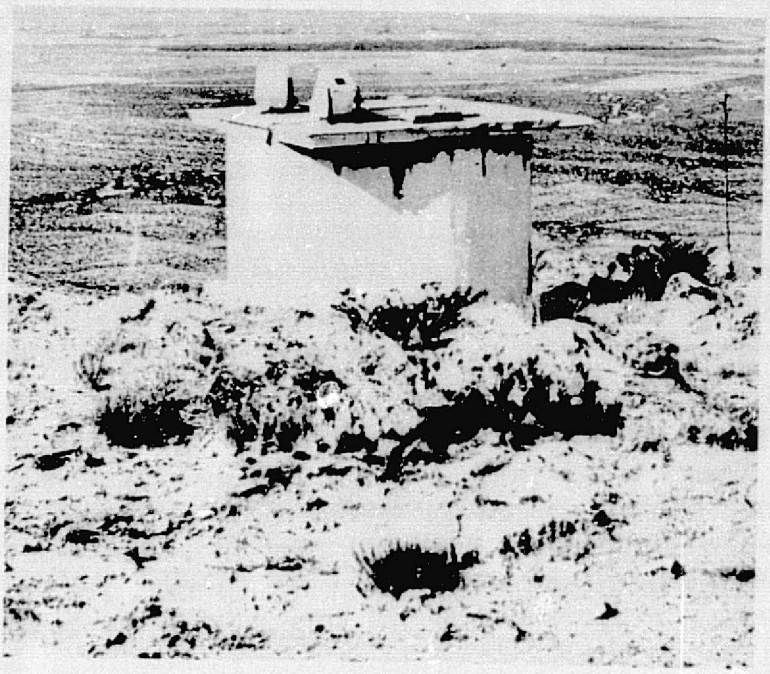

FIGURE 1. METEOR OBSERVATORY, TORTUGAS STATION.

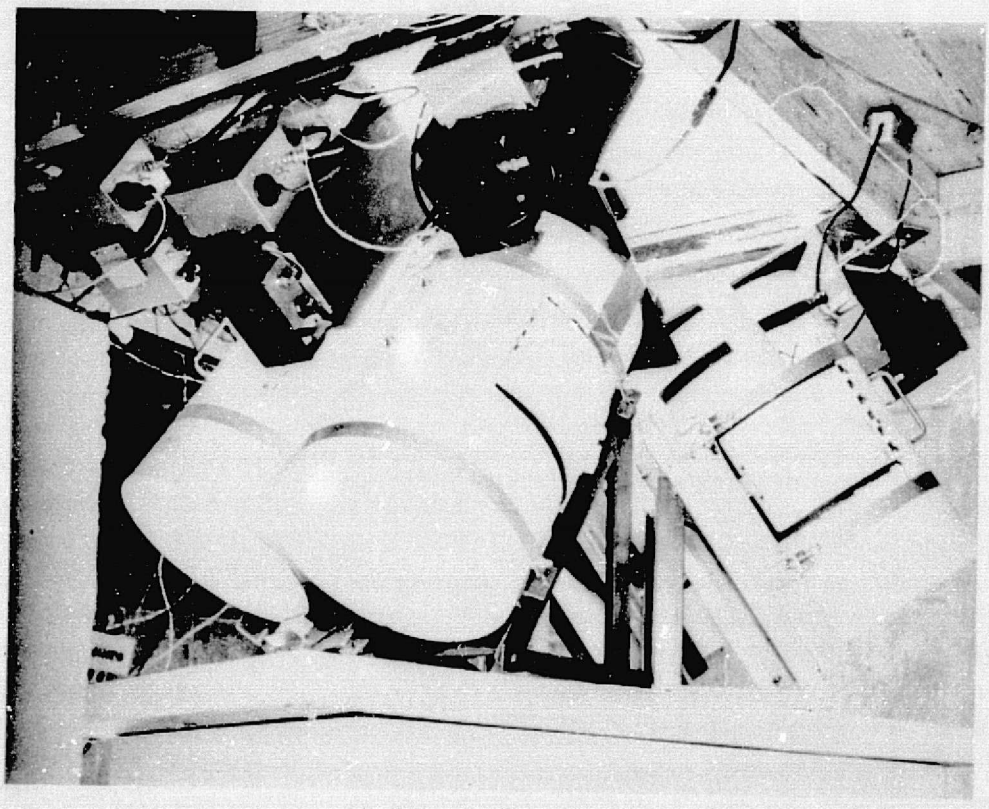

FIGURE 2. METEOR SPECTROGRAPHS, TORTUGAS STATION.

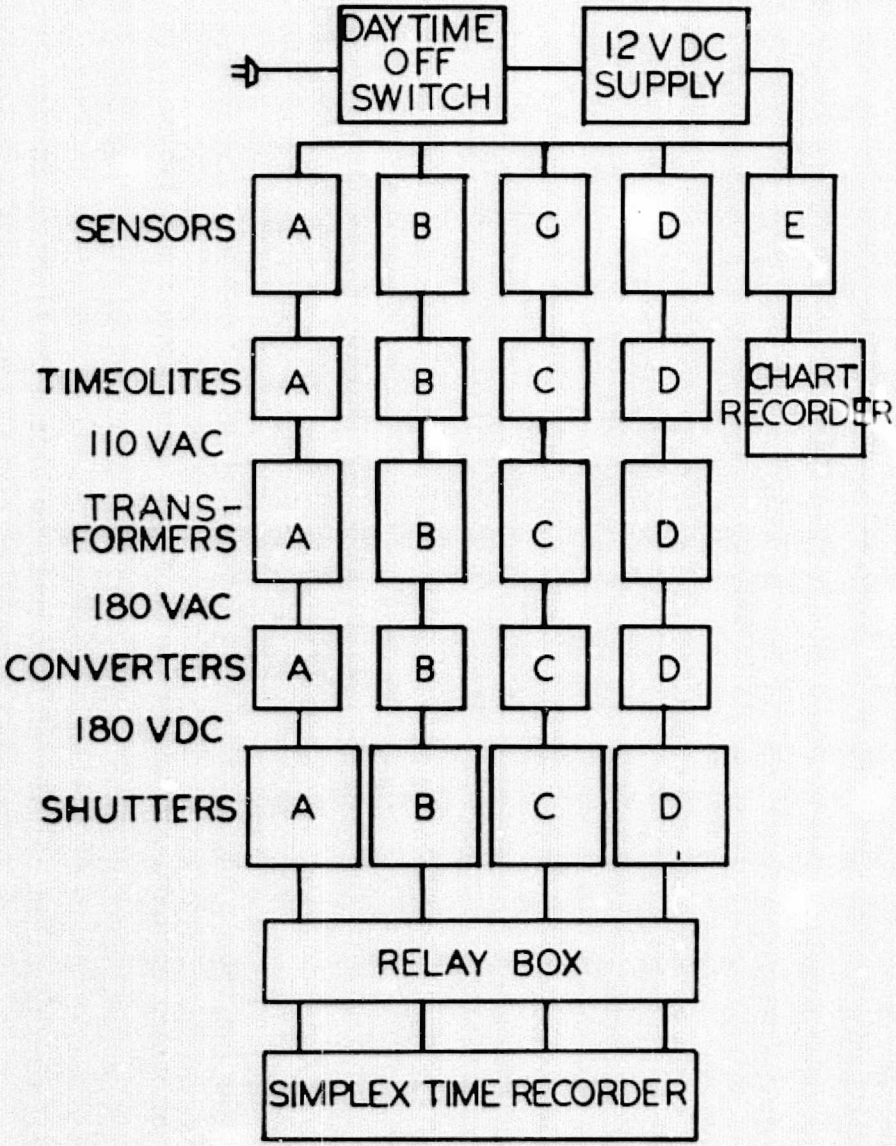

FIGURE 3. WIRING SCHEMATIC, SPECTROGRAPHS, METEOR STATION.

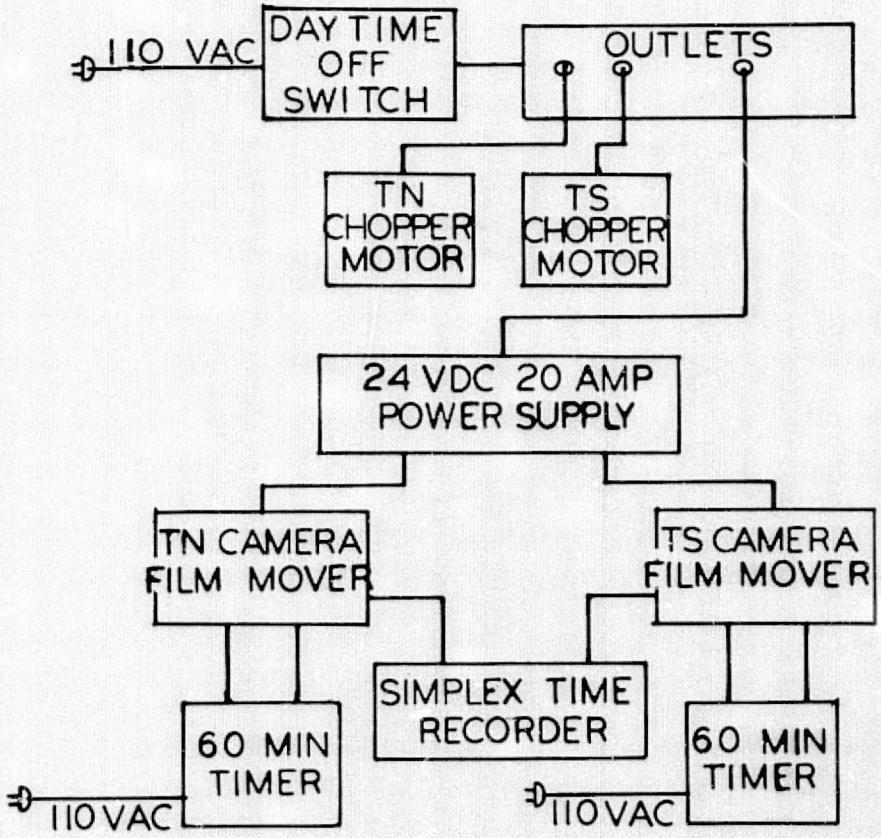

FIGURE 4. WIRING SCHEMATIC OF TWO STATION METEOR PATROL CAMERAS.

MEASUREMENTS OF JUPITER'S LONG-LIVED FEATURES AND CURRENTS

E. J. Reese and R. F. Beebe

Department of Astronomy

New Mexico State University, Las Cruces, New Mexico

Recent longitudinal measurements of Jupiter's Red Spot are presented to illustrate the constancy of the 90-day oscillation. Observational parameters of the Red Spot, the three south temperate ovals, and a summary of the zenographic latitudes of the belts are tabulated for the time interval from 1972 to 1975. Drift rates and the mean latitudes of the atmospheric currents for the 1974-75 apparition are presented.

INTRODUCTION

Since we have not published detailed apparitional reports during the interval from 1972 to 1976, this report summarizes the general parameters of the Jovian atmosphere for that time interval. The current efforts of the NMSU group are directed toward a much more extensive measuring program, with the goal of obtaining detailed information on growth and drift rates of short-lived features as well as continuing analysis of the long-lived features.

During the period from 1972 to 1976 an automated measuring program has been implemented, resulting in the capacity to obtain positional information on all observed features in the Jovian atmosphere. Requests concerning detailed results of this program should be directed to the authors.

The data reduction procedure utilized in this report is discussed by Solberg (1969). The automation has led to few changes in the procedure but has greatly enhanced the speed and accuracy with which the data are recorded and reduced from plate coordinates to planetographic coordinates. The reduction procedure is an interactive approach, which allows for considerable logical decision on the part of the user.

The following sections discuss the observational aspects and motions of the Red Spot and south temperate ovals, as well as the rotational rates of the atmospheric currents and the latitudinal dependence of the belts.

THE CHANGING ASPECT OF JUPITER'S GREAT RED SPOT

Historically, Jupiter's great Red Spot has displayed two characteristic aspects: the Red Spot or dark aspect, and the Red Spot Hollow or bright aspect. The Red Spot achieved maximum darkness in 1878-1882, 1927, 1936-1937, 1961-1966, and 1969-1974; while the Red Spot Hollow was bright in 1831, 1897, 1930, 1938, 1944, 1947-1948, 1950, 1953-1954, and 1958-1959. Occasionally this famous region assumes an intermediate aspect in which a diffuse, dusky Red Spot is visible within a rather dull Hollow. Such an aspect persisted during 1967 and early 1968.

Prior to 1962, the outbreak of a major SEB disturbance invariably was followed in two or three months by a fading of the Red Spot and the formation of the Hollow. The SEB disturbances of 1962, 1964, and 1971, however, were not followed by a great loss in the intensity of the Red Spot. Perhaps the unusual darkness of the Red Spot during those years enabled it to survive; or, perhaps, much of the energy of the disturbances was diverted into the Equatorial Zone which was unusually dark and orange in color subsequent to each of these disturbances.

The latest SEB disturbance erupted in early July 1975. This time the Red Spot appears to be fading and changing into the Red Spot Hollow aspect. Prior to July, the Red Spot was very dark orange in color and well-defined, contrasting strongly with the brilliant blue-white South Tropical Zone--a typical pre-disturbance aspect. Dark material, which had been moving away from the center of the SEB disturbance along the SEBs, arrived at the preceding end of the Red Spot on 13 September. Thereafter, the Red Spot gradually faded and became more diffuse until by mid-December it had dwindled to half its former area. Its aspect was then similar to that observed in 1967. In blue and green light the Red Spot was visible as a diffuse, dusky patch inside the dark border of the developing Hollow; while in red light the interior of the Hollow was bright and had a well-defined dark border.

Prior to mid-July 1975 the Red Spot had a length of 27,000 km and a width of 14,300 km. By mid-December the dimensions of the faded Red Spot were only 20,500 km by 9,300 km, while the bright interior of the Hollow as photographed in red light was 24,500 km by 13,300 km.

In early February 1976 it became apparent that the disturbance in the SEB was weakening and the Red Spot was recovering some of its former intensity and size.

RED SPOT'S MOTION IN LONGITUDE

After a sudden acceleration in the rotational velocity of the Red Spot in late December 1970 (Reese, 1972a), a gradual deceleration characterized the long-term motion of this famous feature until the end of 1973. The velocity was constant, except for the effects of the 90-day oscillation, during the apparition of 1974-75. The Red

Spot was accelerating again during the apparition of 1975-76. The observed accelerations expressed in units of 10^{-8} m/sec^2 were -3.16 in 1971, -2.42 in 1972, -1.03 in 1973, zero in 1974-75, and +4.10 in 1975-76. Fig. 1 shows the Red Spot's motion in longitude from 1970 to 1975.

The 90-day oscillation in the longitude of the Red Spot (Solberg, 1969) continued throughout the interval covered by this report (Fig. 2 and Table I). Fifty-four complete oscillations have been observed (or extrapolated between the maxima of 16 August 1962 and 1 December 1975. A least squares analysis gives the oscillation a mean period of 89.85 ±0.06 days and an amplitude of 0°.8.

MEASUREMENT OF THE RED SPOT AND THE THREE S. TEMPERATE OVALS

Some values obtained from our measurements of the size and position of the Red Spot and three bright south temperate ovals during the last four apparitions are summarized in Tables II through V. The results for 1975-76 are preliminary since the apparition was still in progress when this report was being prepared.

All of the measurements of the Red Spot and the three south temperate ovals reported here were made on plates taken in blue light. Measurements of plates taken in red light make the lengths of the south temperate ovals about 1°.4 greater at that wavelength.

ATMOSPHERIC CURRENTS IN 1974-75

The zenographic coordinates of the preceding, following, north and south edges of 3,664 spots on 736 plates have been measured for the apparition of 1974-75. A preliminary analysis of these measurements has been completed and a catalog giving basic information concerning 184 identified

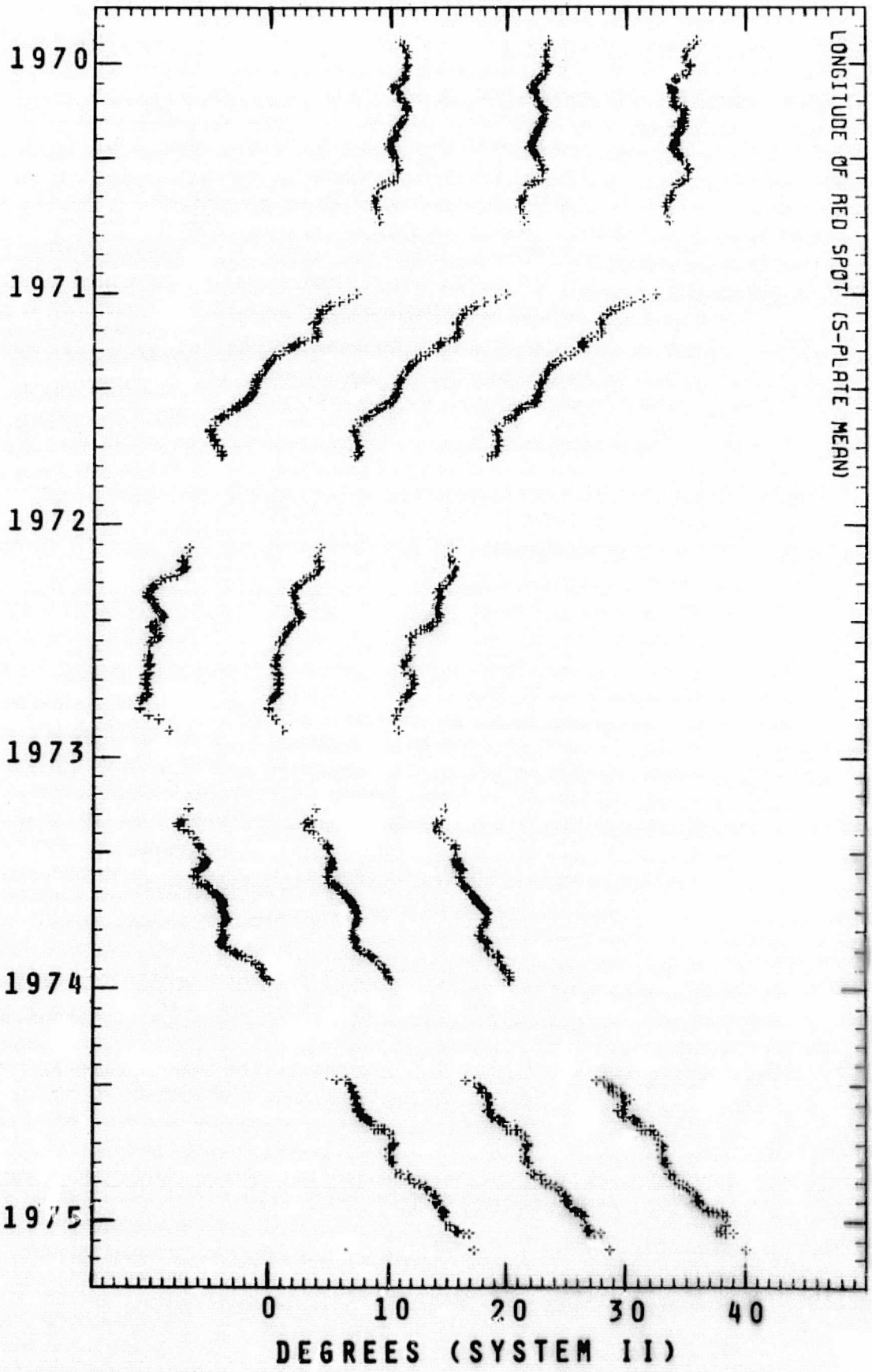

Fig. 1. Longitude of the preceding end, center, and following end of Jupiter's Red Spot, 1970-1975, five-point running means.

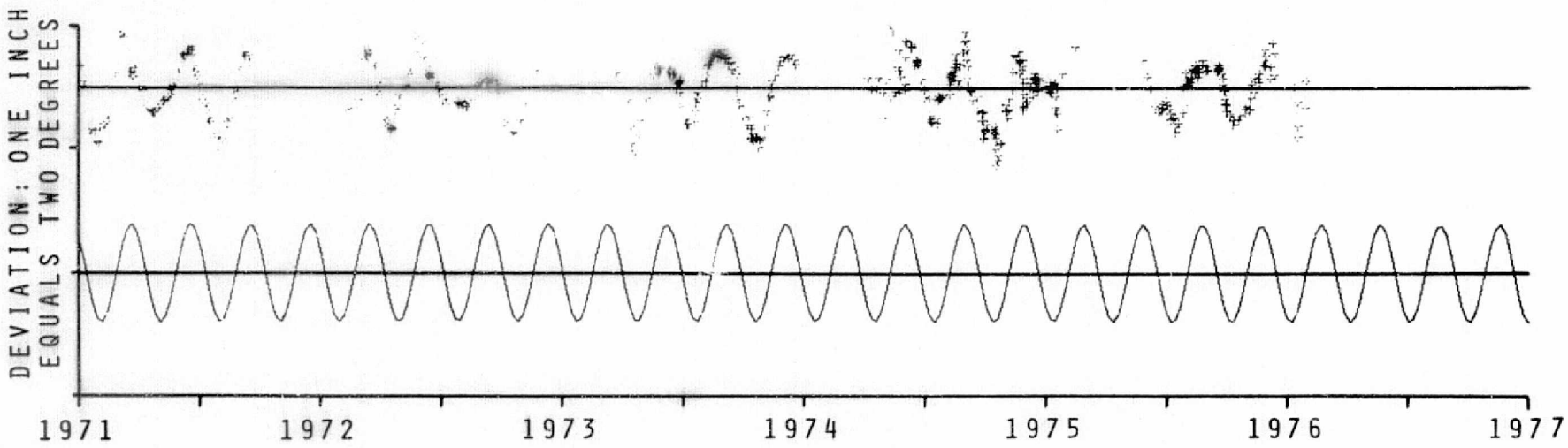

Fig. 2. The Red Spot's 90-day oscillation in longitude from January 1971 to February 1976. In the upper part of the graph, measured longitudes of the center of the Red Spot are plotted as deviations from a least squares fit for each of the five apparitions. The apparition of 1974-75 required only a linear solution; the apparitions of 1971, 1972, 1973-74 and 1975-76 required second degree solutions. The bottom curve shows the predicted oscillation based on a least squares analysis of data from August 1962 to September 1970.

TABLE I

OBSERVED MAXIMA AND MINIMA OF
RED SPOT'S OSCILLATION IN LONGITUDE

Event number	Observed calendar date	Observed Julian date*	Computed Julian date*	$\Delta\lambda$
69	6 Feb 72	1354	1344	-0°8
70	11 Mar 72	1388	1389	+0.6
71	15 Apr 72	1423	1434	-0.7
72	25 May 72	1463	1479	+1.0
73	22 Jul 72	1521	1524	-0.4
74	8 Sep 72	1569	1569	+0.3
75	16 Oct 72	1607	1614	-0.8
76	7 Dec 72	1659	1659	+0.9
78	13 Mar 73	1755	1749	+0.9
79	19 Apr 73	1792	1793	-1.0
80	3 Jun 73	1837	1838	+0.5
81	10 Jul 73	1874	1883	-0.7
82	26 Aug 73	1921	1928	+0.6
83	19 Oct 73	1975	1973	-1.0
84	7 Dec 73	2024	2018	+0.6
87	9 Apr 74	2147	2153	-0.8
88	2 Jun 74	2201	2198	+0.7
89	15 Jul 74	2244	2243	-0.8
90	21 Aug 74	2281	2288	+0.8
91	8 Oct 74	2329	2333	-0.8
92	30 Nov 74	2382	2377	+0.4
93	14 Jan 75	2427	2422	-0.5
94	28 Feb 75	2472	2467	+0.8
96	10 Apr 75	2543	2557	+0.7
97	7 Jul 75	2601	2602	-0.7
98	24 Aug 75	2649	2647	+0.6
99	17 Oct 75	2703	2692	-0.6
100	1 Dec 75	2748	2737	+0.5

*Add 2,440,000

TABLE II

RED SPOT AND SOUTH TEMPERATE OVALS, 1972

Date of Opposition: 24 Jun 72

Red Spot:

Mean rotation period during apparition = $9^h55^m40^s.10 \pm 0^s.04$
Mean drift rate = -0.0130 ± 0.0010°/day (Sys II) = -3.41 ± 0.02 m/sec (Sys III-65)
Equation of position for axis of oscillation:

$$\lambda_2 = 6.987 - 0.04438\ x + 0.0000764\ x^2 \qquad [x = \text{JD } 2441293]$$

Acceleration = -2.4×10^{-8} m/sec^2
Longitude of center at opposition = 1°.2 (Sys II)
Mean latitude of center = -22°.67 ± 0°.07 (50 dates)
Mean length = 23°.37 ± 0°.15 = 27,182 ± 174 km (78 dates)
Mean width = 11°.92 ± 0°.11 = 13,321 ± 123 km (50 dates)

FA:

Mean rotation period = $9^h55^m17^s.38 \pm 0^s.07$
Mean drift rate = -0.5666 ± 0.0018°/day (Sys II) = +3.71 ± 0.02 m/sec (Sys III-65)
Longitude of center at opposition = 343°.3 (Sys II)
Mean latitude of center = -32°.80 (10 dates)
Mean length = 12°.36 ± 0°.19 = 13,221 ± 210 km (52 dates)
Mean width = 6°.90 = 7,960 km (9 dates)

BC:

Mean rotation period = $9^h55^m15^s.18 \pm 0^s.06$
Mean drift rate = -0.6202 ± 0.0014°/day (Sys II) = +4.37 ± 0.02 m/sec (Sys III-65)
Longitude of center at opposition = 55°.2 (Sys II)
Mean latitude of center = -32°.64 (5 dates)
Mean length = 12°.73 ± 0°.19 = 13,636 ± 206 km (49 dates)
Mean width = 7°.25 = 8,359 km (5 dates)

DE:

Mean rotation period = $9^h55^m16^s.41 \pm 0^s.12$
Mean drift rate = -0.5903 ± 0.0028°/day (Sys II) = +4.00 ± 0.03 m/sec (Sys III-65)
Longitude of center at opposition = 193°.9 (Sys II)
Mean latitude of center = -32°.92 (4 dates)
Mean length = 12°.96 ± 0°.24 = 13,846 ± 264 km (30 dates)
Mean width = 7°.72 = 8,909 km (4 dates)

Conjunction of FA and RS: 1972, May 22.2, λ_2 = 2°.1

Conjunction of BC and RS. 1972, Sep 20.5, λ_2 = 0°.6

TABLE III

RED SPOT AND SOUTH TEMPERATE OVALS, 1973-74

Date of Opposition: 30 Jul 73

Red Spot:

Mean rotation period during apparition = $9^h55^m41^s.58 \pm 0^s.03$
Mean drift rate = +0.0230 0.008°/day (Sys II) = -3.89 ± 0.01 m/sec (Sys III-65)
Equation of position for axis of oscillation:

$$\lambda_2 = 2.777 + 0.008623\ x + 0.0000331\ x^2 \quad [x_0 = \text{JD } 2441694]$$

Acceleration = -1.03×10^{-8} m/sec^2
Longitude of center at opposition = 5°.9 (Sys II)
Mean latitude of center = -22°.24 ± 0°.06 (26 dates)
Mean length = 21°.73 ± 0°.09 = 25,345 ± 111 km (97 dates)
Mean width = 12°.02 ± 0°.09 = 13,420 ± 101 km (26 dates)

FA:

Mean rotation period during apparition = $9^h55^m16^s.28 \pm 0^s.09$
Mean drift rate = -0.5933 ± 0.0021°/day (Sys II) = +4.04 ± 0.03 m/sec (Sys III-65)
Longitude of center at opposition = 112°.5 (Sys II)
Mean latitude of center = -32°.84 ± 0°.11 (8 dates)
Mean length = 10°.8 ± 0°.2 = 11,548 ± 171 km (32 dates)
Mean width = 6°.7 ± 0°.3 = 7,730 ± 378 km (8 dates)

BC:

Mean rotation period = $9^h55^m16^s.30 \pm 0^s.07$
Mean drift rate = -0.5929 ± 0.0016°/day (Sys II) = +4.03 ± 0.02 m/sec (Sys III-65)
Longitude of center at opposition = 175°.4 (Sys II)
Mean latitude of center = -32°.80 ± 0°.16 (12 dates)
Mean length = 11°.3 ± 0°.2 = 12,088 ± 172 km (38 dates)
Mean width = 7°.3 ± 0°.2 = 8,421 ± 186 km (12 dates)

DE:

Mean rotation period = $9^h55^m15^s.07 \pm 0^s.11$
Mean drift rate = -0.6229 ± 0.0028°/day (Sys II) = +4.40 ± 0.03 m/sec (Sys III-65)
Longitude of center at opposition = 312°.9 (Sys II)
Mean latitude of center = -32°.43 ± 0°.21
Mean length = 12°.0 ± 0°.4 = 12,886 ± 481 km (24 dates)
Mean width = 7°.0 ± 0°.2 = 8,065 ± 237 km (9 dates)

Conjunction of DE and RS: 1973, May 9.6, λ_2 = 4°.1

Conjunction of FA and RS: 1974, Jan 17.7, λ_2 = 10°.4

TABLE IV

RED SPOT AND SOUTH TEMPERATE OVALS, 1974-75

Date of Opposition: 5 Sep 74

Red Spot:

Mean rotation period during apparition = $9^h55^m42^s.49 \pm 0^s.03$
Mean drift rate = +0.0453 ± 0.0008°/day (Sys II) = -4.20 ± 0.01 m/sec (Sys III-65)
Equation of position for axis of oscillation:

$$\lambda_2 = 12.421 + 0.045329\ x \qquad [x_0 = \text{JD } 2442096]$$

Longitude of center at opposition = 21°.6 (Sys II)
Mean latitude of center = -21°.94 ± 0°.03 (163 dates)
Mean length = 22°.68 ± 0°.10 = 26,218 ± 117 km
Mean width = 12°.74 ± 0°.06 = 14,208 ± 67 km

FA:

Mean rotation period = $9^h55^m17^s.7 \pm 0^s.1$
Mean drift rate = -0.5690 ± 0.0017°/day (Sys II) = +3.73 ± 0.02 m/sec (Sys III-65)
Longitude of center at opposition = 238°.4 (Sys II)
Mean latitude of center = -33°.16 ± 0°.07 (105 dates)
Mean length = 12°.78 ± 0°.17 = 13,615 ± 181 km
Mean width = 7°.62 ± 0°.08 = 8,802 ± 93 km

BC:

Mean rotation period = $9^h55^m16^s.2 \pm 0^s.1$
Mean drift rate = -0.5945 ± 0.0011°/day (Sys II) = +4.05 ± 0.02 m/sec (Sys III-65)
Longitude of center at opposition = 295°.1 (Sys II)
Mean latitude of center = -33°.29 ± 0°.06 (124 dates)
Mean length = 13°.08 ± 0°.14 = 13,920 ± 149 km
Mean width = 7°.90 ± 0°.08 = 9,128 ± 92 km

DE:

Mean rotation period = $9^h55^m15^s.7 \pm 0^s.1$
Mean drift rate = -0.6081 ± 0.0011°/day (Sys II) = +4.22 ± 0.02 m/sec (Sys III-65)
Longitude of center at opposition = 68°.6 (Sys II)
Mean latitude of center = -33°.26 ± 0°.06 (123 dates)
Mean length = 13°.33 ± 0°.13 = 14,186 ± 138 km
Mean width = 7°.77 ± 0°.09 = 8,278 ± 104 km

Conjunction of BC and RS: 1974, Apr 23.4, λ_2 = 15°.3

Conjunction of DE and RS: 1974, Nov 15.4, λ_2 = 24°.6

TABLE V

RED SPOT AND SOUTH TEMPERATE OVALS, 1975-76

Date of Opposition: 13 October 75

Red Spot:

Mean rotation period during apparition = $9^h55^m42^s.60 \pm 0^s.06$
Mean drift rate = +0.0478 ± 0.0015°/day (Sys II) = -4.23 ± 0.02 m/sec (Sys III-65)
Equation of position for axis of oscillation:

$$\lambda_2 = 30.898 + 0.09259\ x - 0.0001339\ x^2 \qquad [x_0 = \text{JD } 2442499]$$

Acceleration = $+4.2 \times 10^{-8}$ m/sec^2
Longitude of center at opposition = 43°.6 (Sys II)
Mean latitude of center = -21°.80 ± 0°.04
Mean length = 21°.89 ± 0°.09 = 25,603 ± 105 km (92 plates)
Mean width = 12°.13 ± 0°.07 = 13,524 ± 78 km (92 plates)

FA:

Mean rotation period = $9^h55^m16^s.12 \pm 0^s.13$
Mean drift rate = -0.5973 ± 0.0031°/day (Sys II) = +4.09 ± 0.04 m/sec (Sys III-65)
Longitude of center at opposition = 0°.3 (Sys II)
Mean latitude of center = -33°.28 ± 0°.08 (69 plates)
Mean length = 12°.54 ± 0°.16 = 13,345 ± 170 km (69 plates)
Mean width = 6°.65 ± 0°.09 = 7,684 ± 104 km (69 plates)

BC:

Mean rotation period = $9^h55^m16^s.56 \pm 0^s.10$
Mean drift rate = -0.5865 ± 0.0025°/day (Sys II) = +3.95 ± 0.03 m/sec (Sys III-65)
Longitude of center at opposition = 57°.3 (Sys II)
Mean latitude of center = -32°.53 ± 0.07 (76 plates)
Mean length = 12°.65 ± 0°.16 = 13,541 ± 172 km (76 plates)
Mean width = 6°.50 ± 0.08 = 7,491 ± 92 km (76 plates)

DE:

Mean rotation period = $9^h55^m15^s.97 \pm 0^s.12$
Mean drift rate = -0.6009 ± 0.0029°/day (Sys II) = +4.13 ± 0.04 m/sec (Sys III-65)
Longitude of center at opposition = 189°.0 (Sys II)
Mean latitude of center = -33°.00 ± 0°.10 (47 plates)
Mean length = 12°.29 ± 0°.17 = 13,120 ± 181 km (47 plates)
Mean width = 6°.34 ± 0°.11 = 7,318 ± 127 km (47 plates)

Conjunction of FA and RS: 1975, Aug 7.2, λ_2 = 40°.8

Conjunction of BC and RS: 1975, Nov 3.8, λ_2 = 44°.7

---

spots distributed in twenty atmospheric currents is now available. The mean latitude and rotation period of the spots in each current is given in Table VI. The total number of spots indicated in Table VI exceeds 184 because in several cases the rotational velocity of a feature changed suddenly and the drift was divided into two sections, each section being more linear than the whole.

Fourteen spots observed near the middle of the North Equatorial Belt are especially interesting since they appeared to originate near a common source having a rotational velocity somewhat greater than System III-65[1]. This apparent source was still active during the apparition of 1975-76.

It is rather interesting to note that the three long-lived south temperate ovals are now rotating about 1 m/sec faster than the mean of five other spots in the S. Temperate Current. It may be very significant that the five spots in the S. Temperate Current have a mean rotation period of $9^h55^m20^s.1$ which was a typical value for this current prior to 1940 when the three long-lived ovals made their first appearance.

A decided correlation between the latitude of spots and their rotational velocity was apparent in the S.S. Temperate Current. Thirteen spots near zenographic latitude -38°.7 had a mean rotation period of $9^h55^m3^s.9$ while eleven spots near latitude -40°.6 had a mean period of $9^h55^m6^s.6$. The spots in the higher latitude were rotating about 1 m/sec more slowly than those in the lower latitude.

---

[1]System III-65, as proposed at IAU Colloquium 30, has a daily motion of 870°.536.

TABLE VI

JUPITER, 1974-75

ATMOSPHERIC CURRENTS

Current	Sys.	No. of spots	Mean β"	Sys. I or II Drift (°/d)	9^h + Period	Sys. III (65) Drift (m/sec)
N. Polar Current	2	3	+50°9	+0.0693	55^m43^s5	- 3.18
N.N.N. Temp. Current	2	6	+44.4	-0.5978	55 16.1	+ 3.53
N.N. Temp. Current-A	2	9	+40.1	-0.1765	55 33.4	- 1.02
N.N. Temp. Current-B	2	4	+35.3	-2.6623	53 51.6	+ 28.84
N. Temp. Current-A	2	10	+32.4	+0.8396	56 15.1	- 13.72
N. Trop. Current-A	2	18	+18.5	-0.3819	55 25.0	+ 1.60
N. Trop. Current-B	2	7	+18.4	-0.8087	55 7.5	+ 7.48
mid-NEB	2	14	+12.5	-3.5517	53 15.4	+ 46.4
N. Equatorial Current-A	1	31	+ 5.5	-0.0480	50 28.1	+106.4
N. Equatorial Current-B	1	17	+ 5.1	+0.5201	50 51.0	+ 98.4
N. Equatorial Current-C	1	27	+ 5.7	-0.4916	50 10.2	+112.8
Central Equat. Current	1	11	+ 1.2	-0.2851	50 18.5	+110.3
S. Equatorial Current-A	1	1	- 5.3	-0.0109	50 29.6	+106.0
S. Equatorial Current-B	1	2	- 5.2	+0.4952	50 50.0	+ 98.7
Red Spot	2	1	-21.9	+0.0453	55 42.5	- 4.20
S. Temp. Belt	2	6	-30.2	-0.5716	55 17.2	+ 3.87
S. Temp. Current	2	5	-32.4	-0.4994	55 20.1	+ 2.90
S. Temp. Ovals:FA,BC,DE	2	3	-33.3	-0.5872	55 16.5	+ 3.95
S.S. Temp. Current	2	24	-39.6	-0.8658	55 5.1	+ 6.85
S.S. Temp. Zone	2	2	-50.6	-0.0779	55 37.4	- 1.79

ZENOGRAPHIC LATITUDES OF JUPITER'S BELTS

The measured latitudes of Jupiter's belts for the apparitions of 1972, 1973, and 1974-75 are summarized in Table VII. A comparison of these measurements with those reported for the apparition of 1971 (Reese, 1971) and the interval from 1960 to 1970 (Reese, 1972b) clearly demonstrates the rather narrow range in latitudes of Jupiter's belts.

The north edge of the North Equatorial Belt and both edges of the North Temperate Belt attained maximum displacements towards the equator during 1971.

We usually measure the latitudes of the belts on photographs taken in blue light; however, a considerable number of measurements are made on photographs taken in red light for comparison purposes. Usually there is little difference between the measured latitudes at these wavelengths; however, the extremely faint south component of the South Equatorial Belt was a notable exception to this rule in 1974-75. In blue light there was one faint belt extending from -17°.6 to -21°.2, while in red light there were two faint belts with one extending from -15°.1 to -17°.5 and the other from -20°.5 to -22°.9.

SUMMARY

This report is directed toward updating information of the form previously presented by Reese (1972a, 1972b). More detailed analysis of various aspects of the data is underway and will be published as individual articles in various journals. In the future a bibliography of articles utilizing our data will be included in this publication.

TABLE VII

ZENOGRAPHIC LATITUDES OF JUPITER'S BELTS

	19 Feb 72 - 30 Apr 72		26 Jun 73 - 16 Oct 73			14 Jul 74 - 19 Jan 75		
	β"	N	β"	σ	N	β"	σ	N
NPB			+53°9	---	1	+57°3	±0°4	11
NNNTB	+45°9	3	+44.7	±0°3	3	+44.2	0.1	23
NNTB	+37.5	17	+37.5	0.6	7	+36.1	0.2	23
N. edge NTB	+30.2	2	+32.0	0.3	7	+30.7	0.2	23
N. edge NTBs	+27.2	21	+27.0	0.1	5	+25.5	0.4	16
S. edge NTB	+22.6	21	+23.8	0.1	7	+24.1	0.3	30
N. edge NEB	+17.7	15	+18.4	0.2	7	+18.5	0.2	24
S. edge NEB	+ 5.6	10	+ 7.5	0.2	7	+ 7.3	0.3	25
N. edge EB	+ 0.3	7	+ 0.7	0.1	6	0.0	0.2	24
S. edge EB	- 3.4	7	- 3.2	0.1	6	- 3.9	0.2	24
N. edge SEBn	- 6.4	8	- 6.8	0.2	7	- 7.2	0.1	24
S. edge SEBn	-10.1	8	-10.7	0.1	7	-10.4	0.1	24
N. edge SEBs	-15.9	12	-16.1	0.2	7	-17.7	0.4	31
S. edge SEBs	-20.0	16	-20.3	0.2	7	-20.7	0.3	31
N. edge STB	-26.7	18	-25.9	0.2	7	-27.1	0.2	25
STB	-29.9	18	-29.4	0.1	7	-30.1	0.2	25
S. edge STB	-33.0	18	-32.8	0.2	7	-33.0	0.2	25
STeZB	-37.2	3	-37.3	0.7	3	-37.6	0.2	16
SSTB	-44.8	11	-44.6	0.9	4	-45.2	0.4	19
SSSTB	-56.1	3	-55.4	0.2	3	-55.9	0.4	18
SPBn	-60.8	2	-----	---	-	-62.9	1.6	3
SPBs	-65.9	3	-64.9	0.2	4	-65.7	0.2	10
N. edge bright S.Cap	-----	-	-68.3	0.5	4	-68.5	0.2	13
N. edge dark EZ	+ 9.5	13						
S. edge dark EZ	-9.7	13						

ACKNOWLEDGMENTS

We wish to thank A. S. Murrell and C. F. Knuckles for their efforts in maintaining the observing program which obtained the photographic data utilized in this report and Dianne Cress and Lou Ann Youngblood for their assistance in measuring and reducing the data. Special recognition should be given to T. C. Bruce for his highly productive efforts in developing the basic reduction programs.

This research was supported by NASA Grant NGL 32-003-001 and NSF Grant MPS75-03734.

REFERENCES

Reese, E. J., 1971, NMSU Observatory TN-72-42

Reese, E. J., 1972a, Icarus 17, 57.

Reese, E. J., 1972b, Contributions of the Observatory, New Mexico State University, 1, No. 3, 83.

Solberg, H. G., 1969, Planetary and Space Science, 17, 1573.